Front. Optoelectron. 2021, 14(2): 229–251
https://doi.org/10.1007/s12200-021-1121-8

REVIEW ARTICLE

Nanoimprint lithography for high-throughput fabrication of metasurfaces

Dong Kyo OH[1*], Taejun LEE[1*], Byoungsu KO[1*], Trevon BADLOE[1], Jong G. OK (✉)[2], Junsuk RHO (✉)[1,3]

1 Department of Mechanical Engineering, Pohang University of Science and Technology (POSTECH), Pohang 37673, Republic of Korea
2 Department of Mechanical and Automotive Engineering, Seoul National University of Science and Technology (SEOULTECH), Seoul 01811, Republic of Korea
3 Department of Chemical Engineering, Pohang University of Science and Technology (POSTECH), Pohang 37673, Republic of Korea

Abstract Metasurfaces are composed of periodic subwavelength nanostructures and exhibit optical properties that are not found in nature. They have been widely investigated for optical applications such as holograms, wavefront shaping, and structural color printing, however, electron-beam lithography is not suitable to produce large-area metasurfaces because of the high fabrication cost and low productivity. Although alternative optical technologies, such as holographic lithography and plasmonic lithography, can overcome these drawbacks, such methods are still constrained by the optical diffraction limit. To break through this fundamental problem, mechanical nanopatterning processes have been actively studied in many fields, with nanoimprint lithography (NIL) coming to the forefront. Since NIL replicates the nanopattern of the mold regardless of the diffraction limit, NIL can achieve sufficiently high productivity and patterning resolution, giving rise to an explosive development in the fabrication of metasurfaces. In this review, we focus on various NIL technologies for the manufacturing of metasurfaces. First, we briefly describe conventional NIL and then present various NIL methods for the scalable fabrication of metasurfaces. We also discuss recent applications of NIL in the realization of metasurfaces. Finally, we conclude with an outlook on each method and suggest perspectives for future research on the high-throughput fabrication of active metasurfaces.

Keywords nanoimprint, scalable fabrication, large-area metasurface, tailored nanostructure, hierarchical nanostructures

Received November 11, 2020; accepted February 2, 2021

E-mails: jgok@seoultech.ac.kr (J. G. Ok), jsrho@postech.ac.kr (J. Rho)

*These authors contributed equally to this work.

1 Introduction

Metasurfaces composed of two-dimensional arrays of nanostructures, called artificial atoms, exhibit optical properties that do not exist in nature. Generally, they consist of subwavelength meta-atoms ($< \lambda/5$) to avoid diffraction [1–3]. Their extraordinary optical properties can be applied to wavefront modulation, such as beam steering devices [4–6], invisibility cloaks [7,8], and hyperlenses, which can overcome the diffraction limit [9–14]. Moreover, multifunctional metasurfaces have been demonstrated for transmission or reflection type color filters [15–24], and metaholograms [25–33]. Metasurfaces have also been exploited as perfect absorbers [34–42], and other optical modulation applications [43–55] due to their versatile functions. As that nanostructures that make up metasurfaces should have precise dimensions in order to realize high optical performance, more elaborate nanofabrication methods to fabricate them are required.

To fabricate metasurfaces with a resolution of sub-10 nm, electron-beam lithography (EBL) is generally used by directly illuminating a high-voltage electron-beam onto an electron-sensitive resist to create the desired shape [56,57]. Maskless fabrication of EBL allows a high degree of freedom and the short wavelength of electrons enables the realization of high-resolution structures [56,58]. However, EBL requires expensive high-vacuum systems incorporated with a series of magnetic lenses to accurately control the electrons. Therefore, it has low-throughput which limits the mass production of nanostructures. To realize the mass production of metasurfaces, numerous optical nanofabrication methods such as holographic lithography (or interference lithography) [59–65] and plasmonic lithography [66–72] have been investigated. However, these processes have the same inherent shortcomings of optical nanopatterning, such as the diffraction limit, which

drives the pursuit of other advanced nanofabrication techniques [73–75].

In this review, we focus on mechanical nanopatterning methods, nanoimprint lithography (NIL), and review the various NIL techniques which can lead to the high-throughput fabrication of metasurfaces. First, we describe what conventional NIL is, then discuss its applications for metasurfaces using various materials such as metals, dielectrics, and emerging materials. Afterward, progressive NIL manufacturing of large-area and high-resolution nanopatterns will be discussed, followed by practical applications of high-throughput production of metasurfaces. Finally, we will conclude by organizing the NIL methods and suggesting perspectives for future research on the high-throughput fabrication of active metasurfaces.

2 Fabrication of metasurfaces by using conventional NIL

Unlike optical nanopatterning processes, NIL uses simple mechanical steps for fabricating nanostructures, leading to various NIL processes. In general, a hard nanopatterned mold is pressed into a resin made up of polymeric material at constant energy to transfer nanopatterns to the resin. There are two conventional NIL methods, thermal and ultraviolet (UV) NIL. Figure 1(a) shows schematics of these processes. Thermal NIL hardens a thermoplastic polymer resin by applying heat, which has been used to improve the resolution of NIL to 25 nm as shown in Fig. 1(b) [76–78]. UV NIL uses ultraviolet light to solidify the resin and generally has higher productivity due to the simple system and fast response time as it does not require a heat source [79]. Figure 1(c) shows the results of using UV NIL to produce 5 nm nanopatterns and Au nanopatterns with 5 nm gaps through the lift-off process [80]. Besides, flexible molds composed of polymeric materials such as polydimethylsiloxane (PDMS) can be utilized in the NIL process, the so-called soft NIL method [81], which has enabled to fabricate uniform nanopatterns on arbitrary surfaces.

NIL has been with various metals to fabricate metasurfaces for numerous applications in the last decade [82–85]. In particular, gold (Au) has been widely used as materials for the fabrication of metasurfaces using NIL due to its affordability and superior plasmonic properties. An Au-coated nanowell array was manufactured through thermal NIL, UV NIL, and electron-beam evaporation to produce structural color pixels [86]. Figure 2(a) shows photographs under ambient light, a microscope image, and SEM images of the flexible plasmonic color patterns. The colors of the six-petal flower of the fabricated metasurface could be reversibly switched with good optical contrast by turning an electrode on or off. In another application of thermal NIL, a polarization-sensitive tunable absorber metasurface with precise Au nanostructures was fabricated [87]. The exact plasmonic nanostructures achieved absorption over 90% over a broad wavelength band in TE mode, with a drastically reduced absorption in TM mode.

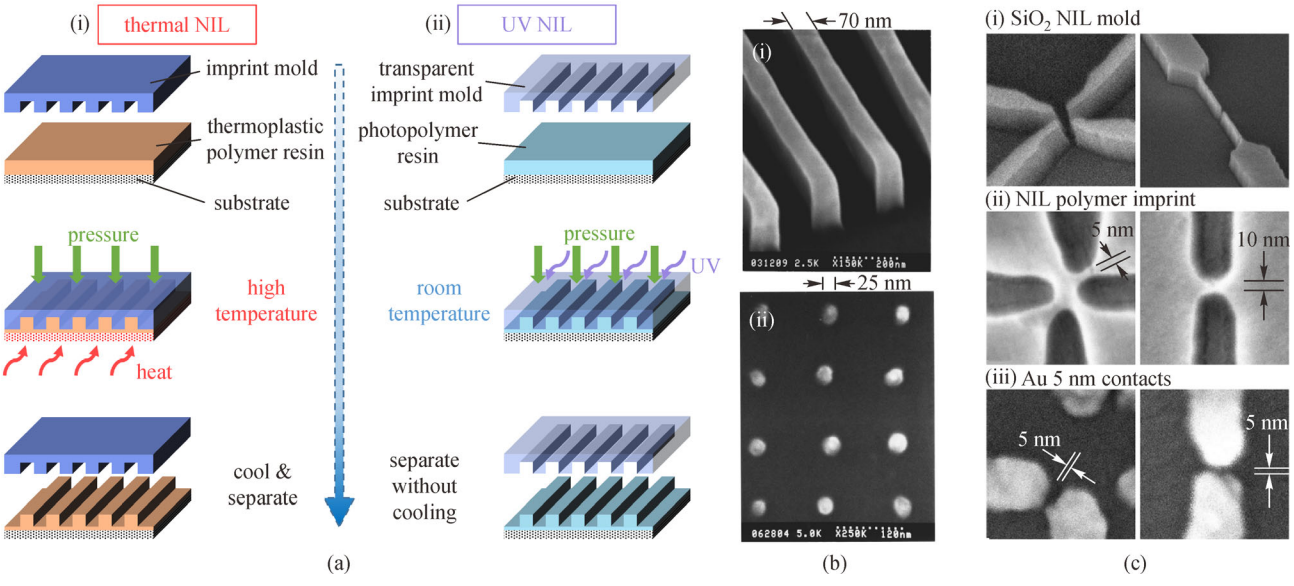

Fig. 1 Conventional nanoimprint lithography (NIL) and its replicating performance. (a) Schematics of (i) thermal NIL and (ii) ultraviolet (UV) NIL. (b) Scanning electron microscope (SEM) images of (i) 70 nm wide and 200 nm tall strips and (ii) 25 nm diameter and 120 nm periodicity metal dots manufactured by thermal NIL. Reprinted with permission from Ref. [76], Copyright 1996, American Institute of Physics. (c) SEM images of (i) a silicon oxide mold, (ii) imprinted resin after UV NIL, and (iii) Au contacts after evaporation of metal and lift-off of the resist, showing 5 nm resolution UV NIL for single-molecule contacts. Reprinted with permission from Ref. [80], Copyright 2004, American Institute of Physics

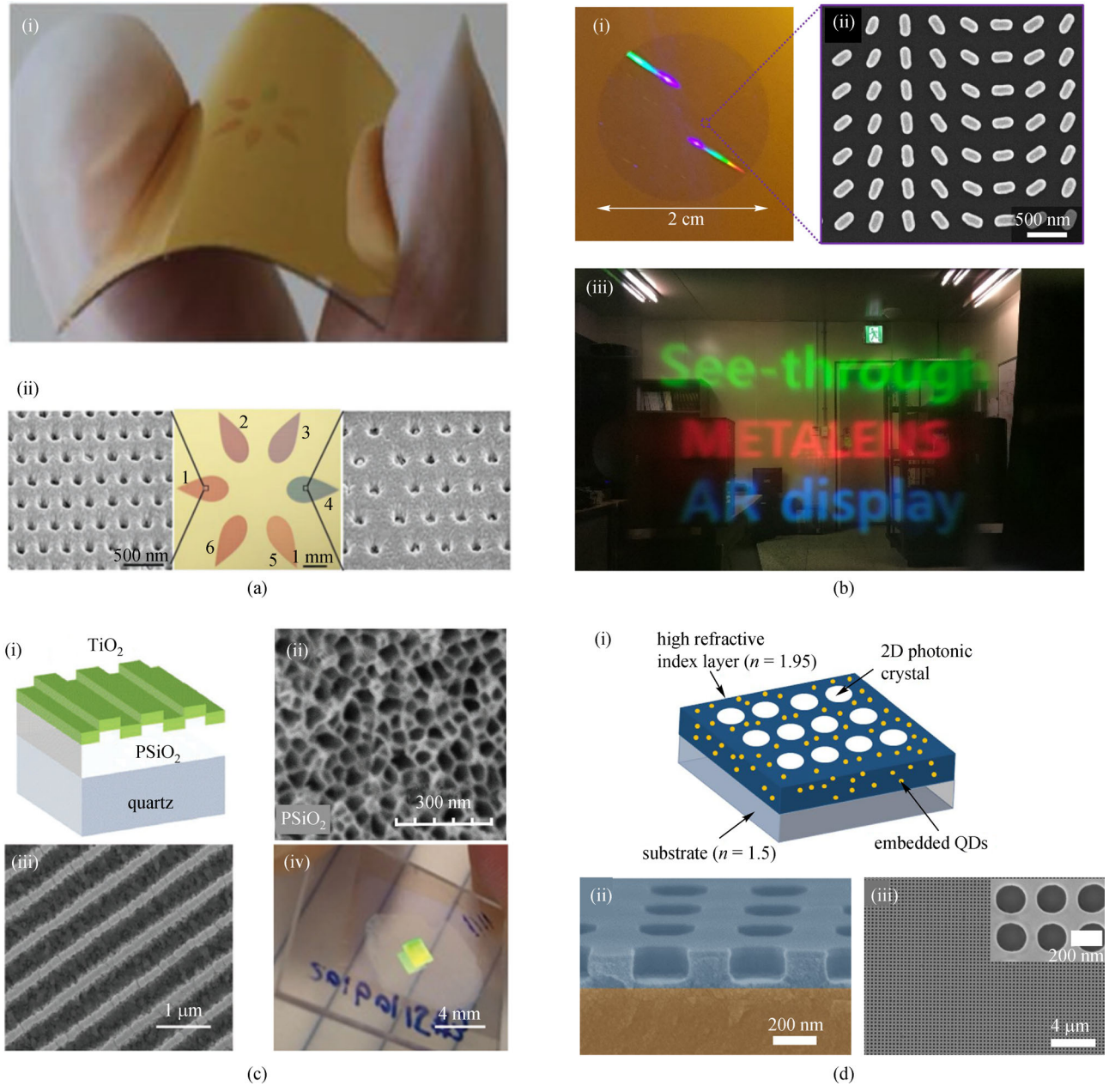

Fig. 2 NIL of various materials for fabrication of metasurfaces. (a) (i) Photograph of a flexible plasmonic color device with gold (Au) and (ii) microscope and SEM images of the device. Reprinted with permission from Ref. [86], Copyright 2018, John Wiley & Sons. (b) (i) Photograph of the fabricated 20 mm diameter metalens with poly-silicon (poly-Si), (ii) SEM image of the device, and (iii) single-color augmented reality (AR) images with real objects for red, green, and blue light. Reprinted with permission from Ref. [91], Copyright 2018, Nature Publishing Group. (c) (i) Schematic of a general photonic crystal sensor, SEM images of (ii) a porous silicon dioxide ($PSiO_2$) film and (iii) the grating nanostructures that generate the photonic crystal resonant mode, and (iv) photograph of the photonic crystal fabricated on a quartz slide. Reprinted with permission from Ref. [92], Copyright 2017, John Wiley & Sons. (d) (i) Schematic, SEM images of (ii) cross and (iii) top view of a photonic device with quantum dots (QDs). Reprinted with permission from Ref. [101], Copyright 2017, Nature Publishing Group

Beyond metal-based metasurfaces, the fabrication of dielectric metasurfaces has been studied extensively through NIL [88–90]. For example, a large-area metalens with a high numerical aperture (NA) was fabricated using poly-silicon (poly-Si) [91]. A polymer stamp was fabricated using UV NIL and evaporated with Au, chromium (Cr), and silicon dioxide (SiO_2). The evaporated layers were transferred to the poly-Si substrate and etched to create the final metalens. Figure 2(b) shows a photograph, SEM image of metalens, and single-color augmented reality (AR) images with real objects. In addition, porous silicon dioxide ($PSiO_2$) structures were nanopatterned using NIL and subsequently titanium dioxide (TiO_2) was deposited to modulate the resonant

mode of a photonic crystal sensor with an ultralow refractive index (n = 1.09) [92]. Figure 2(c) shows an illustrative schematic of the general photonic crystal sensor, SEM images of the $PSiO_2$ and TiO_2 respectively, and a photograph of the photonic crystal fabricated on a quartz slide. By immersing the device in aqueous dimethyl sulfoxide (DMSO) solutions with a concentration from 1% to 20% by volume, a sensitivity of about 502 nm/refractive index unit (RIU) was confirmed.

Emerging exotic materials have been studied using NIL for the fabrication of innovative metasurfaces. Perovskites are an emerging material for metasurfaces due to their many advantages such as high carrier mobility, superior carrier recombination, low number of defects and impurities, and long carrier diffusion lengths [93–96]. To enhance resonant properties, for example, a functional metasurface with halide perovskites was imprinted [97]. The large-scale perovskite metasurface exhibited significantly enhanced photoluminescence (PL) properties of up to 8 times in the visible and near-IR regimes under one-photon photoexcitation and up to 70 times under three-photon photoexcitation. A metasurface made up of a hybrid organohalide perovskite was also fabricated using thermal NIL [98]. Due to the enhanced morphology of the hybrid organohalide perovskite with optical absorption properties, larger grain sizes, and higher crystallinity, amplified emission was observed with an 8-fold enhancement. The fabrication of nanostructures containing quantum dots (QDs) through NIL is another promising application to easily improve the performance of photonic devices [99]. To increase the optical absorption of colloidal quantum dots (CQDs), a CQD film was spin-coated on a nanopatterned PDMS substrate using NIL, showing an enhanced power conversion efficiency (PCE) of 10.1% [100]. Furthermore, a high refractive index (n = 1.95) material integrated with QDs was fabricated using NIL to produce a photonic device with high fidelity and resolution, as shown in Fig. 2(d) [101]. NIL of TiO_2 sol-gels with QDs or coating of a QD/polymer composite film after NIL of the TiO_2 sol-gels improved density of optical states (DOSs) and PL.

Although NIL has been applied to produce metasurfaces using various promising materials, there are still some challenges to overcome for the high-throughput fabrication of metasurfaces, such as low mechanical properties of materials, difficulties of large-area mold fabrication, and strict defect control [89,102]. Facile NIL technologies have been studied actively to achieve this and are described in the next section.

3 Scalable NIL and its fabrication of metasurfaces

Since NIL transfers nanostructures based on a mechanical embossing process, it has been easily developed to fabricate large-area nanostructures. In this section, various technologies for scalable NIL processes and their applications in metasurface fabrication will be discussed. First, roll-to-roll (R2R) NIL processes are discussed, followed by detailed research for continuous R2R NIL processes. Next, alternative NIL technologies beyond R2R NIL will be described. At the end of this section, practical applications of described scalable NIL methods for the large-scale fabrication of metasurfaces will be presented in detail.

3.1 NIL for continuous fabrication of nanostructures

Although conventional NIL can produce large-area nanopatterns, there have been some drawbacks such as nonuniform pressure distribution, and the limitation of a continuous process, due to the plate-to-plate (P2P) transfer mechanism. To solve the problem associated with achieving a conformal contact over a large surface, other sources like electric field has been applied to NIL, but this caused another complex system [103]. As an alternative methodology, R2R NIL was developed, as shown in Fig. 3(a) [104]. A flexible ethylene-tetrafluoroethylene (ETFE) mold was attached to a roller composed of stainless steel and a soft cushion layer for conformal contact during NIL. After a liquid resin was coated on the flexible polyethylene terephthalate (PET) substrate, the resin was continuously imprinted by the spherical ETFE mold and cured by UV light. By using continuous steps in the entire NIL process, high-speed imprinting with 1.3–23.5 mm/s web speed was realized.

Because of the localized uniform contact of R2R NIL, transferring hierarchical nanopatterns is easier than conventional NIL, as demonstrated in Fig. 3(b) [105]. First, a polyurethane acrylate (PUA) resin on a flexible polyimide (PI) substrate was imprinted using the Si mold with hierarchical structures to fabricate a gecko-foot-inspired shape. The fabricated flexible PUA mold was wrapped to a belt-type roller and then the PDMS was coated continuously on the target substrate. The coated PDMS and the flexible PUA mold were faced each other by a thermal roll-imprinting lithography (TRL) system at a temperature of about 130°C for 3 min. Through this process, the gecko-foot-inspired hierarchical nanostructures were fabricated continuously at a high speed of about 2.5 mm/s. Likewise, double-sided R2R NIL which can be used to fabricate micro-nano structures on both sides of a target substrate was also introduced and is shown in Fig. 3(c) [106]. First, a PDMS mold with micropillar structures was fabricated and the mold was imprinted again with a nanopatterned web to achieve hierarchical structures. Next, an array of the flexible mold was integrated into a UV R2R NIL system, contacting the hierarchical mold and the nanopatterned web to each other. Then a UV curable resin was dispersed at the edge of the mold to fill the channel by capillary action and cured with UV light, making the double-sided

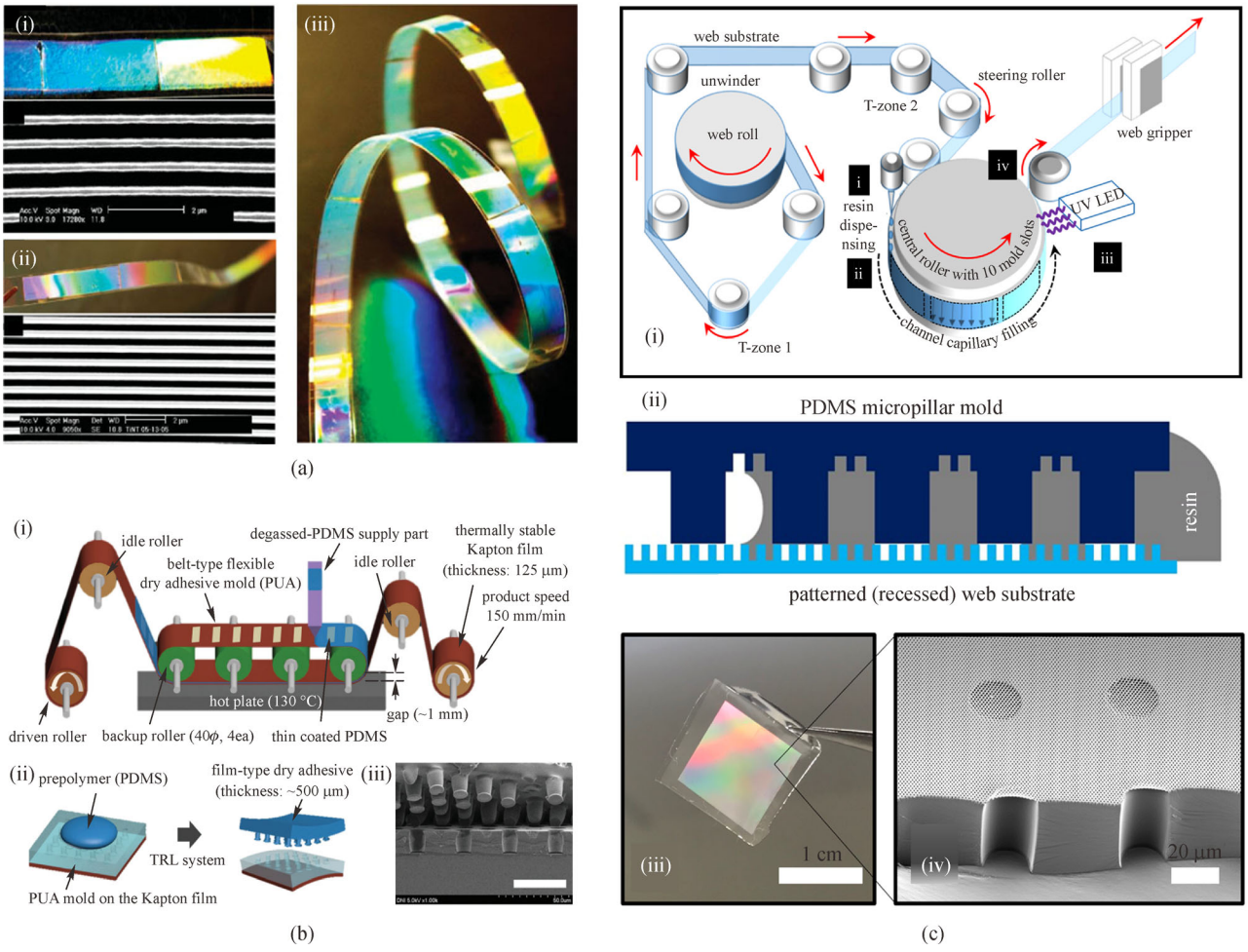

Fig. 3 Continuous NIL methods. (a) (i) Photograph and SEM image of a 700 nm period, 300 nm linewidth grating pattern with polydimethylsiloxane (PDMS) on a polyethylene terephthalate (PET) substrate by using thermal roll-to-roll (R2R) NIL, (ii) and (iii) photograph and SEM image of a 700 nm period, 300 nm linewidth epoxy silicone grating pattern imprinted on a PET strip by using UV R2R NIL. Reprinted with permission from Ref. [104], Copyright 2008, John Wiley & Sons. (b) (i) Schematic of thermal roll-imprinting lithography (TRL) system for scalable fabrication of PDMS with hierarchical nanostructures, (ii) schematic of dispensing and demolding PDMS, and (iii) SEM image of the dry adhesive composed of PDMS. The scale bar is 30 μm. Reprinted with permission from Ref. [105], Copyright 2018, The Royal Society of Chemistry. (c) Schematic of (i) the custom-designed R2R NIL system and (ii) the fabrication of double-sided microporous membranes and (iii) photograph and (iv) SEM image of an imprinted resin after detaching from the mold. Reprinted with permission from Ref. [106], Copyright 2018, American Chemical Society

hierarchical architectures on the membrane substrate continuously.

Besides, continuous post-processing was integrated with R2R NIL to produce complex nanostructures. Continuous silver (Ag) wiring was applied to nanopatterns fabricated by R2R NIL, shown in Fig. 4(a) [107]. The integrated R2R system contains not only the resin imprinting module but also the Ag imprinting module. In this system, the UV resin was imprinted using a flexible nickel (Ni) mold and the Ag paste was subsequently coated, imprinted, and thermally cured on the patterned resin. The sequential process was used to make conformal and large-area Ag electrodes on a flexible PET substrate. The researchers also studied an upgraded R2R system which is combined with double-sided UV R2R NIL [108]. To increase the transmittance of the Ag electrodes on one side, moth-eye nanostructures were fabricated on the other side using double-sided R2R NIL. In addition, a continuous atmospheric-pressure plasma jet (APPJ) process with R2R NIL was also researched [109]. The APPJ provided an alternative approach for the continuous removal of the residual layer after NIL, owing to its advantages such as the process condition in room temperature and atmospheric pressure environment [110]. By removing nanostructures fabricated with UV R2R NIL sequentially and differentially through the continuous APPJ process, a 10.1-inch scale capacitive-type film touch sensor was manufactured consecutively.

However, as attractive as R2R NIL processes are, there are also many challenges, such as experimental errors, poor resin properties, and the absence of fabrication of

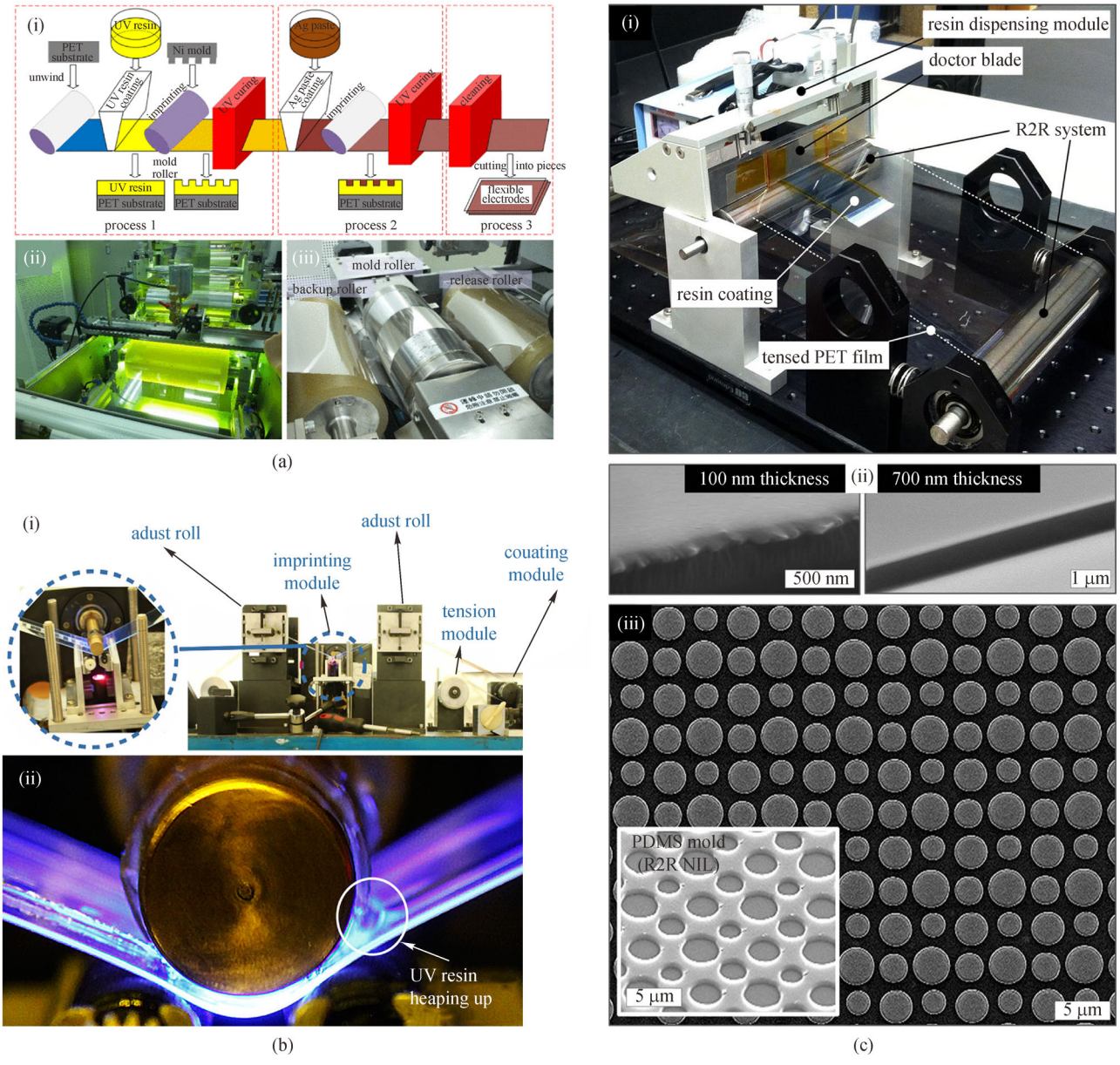

Fig. 4 R2R NIL optimization and analysis for productive fabrication. (a) (i) Schematic of the manufacturing process for flexible electrodes by UV R2R NIL, (ii) the UV R2R NIL system, and (iii) the forming unit. Reprinted with permission from Ref. [107], Copyright 2017, Institute of Electrical and Electronics Engineers. (b) (i) Experimental equipment used for the R2R process and (ii) phenomenon of UV resin accumulation. Reprinted with permission from Ref. [111], Copyright 2017, American Vacuum Society. (c) (i) Photograph of a compact desktop coating system of conformal doctor blading of a resin and R2R feeding module, (ii) microscope images of the doctor-bladed silsesquioxane (SSQ) films on the flexible PET substrate, and (iii) SEM images of nanodot array fabricated on the SSQ film by R2R NIL. The inset to (iii) is the PDMS mold used in R2R NIL. Reprinted with permission from Ref. [116], Copyright 2017, Korea Nano Technology Research Society

large-area flexible molds, so research to solve these problems has been actively conducted. To compensate for experimental errors, the origins of the UV resin accumulation on the filling process in UV R2R NIL was theoretically simulated, as shown in Fig. 4(b) [111]. A numerical study was conducted using the sliding mesh and open-channel flow methods. With increasing the accumulation, the air gap continuously reduced and disappeared under suitable speeds. Another numerical study for the optimization of UV R2R NIL was also conducted [112]. The numerical model based on a single zone with open-channel boundary conditions was proposed and filling the UV resin consequently into the cavity of the mold was analyzed successfully.

Various resins and their properties have also been studied to increase the efficiency of R2R NIL processes

[113,114]. Among them, the conformal coating of silsesquioxane (SSQ) is one example [115]. By using airbrush technology, a thin-film coating was achieved easily, enabling a small residual layer thickness (RLT). The RLT is a crucial parameter for efficient NIL processes because it defines how much resin is wasted, so through modulation of the resin concentration and airbrushing pressure, the film thickness and resulting RLT were readily controllable. As a follow-up study, the airbrushing method was practically applied to continuous R2R NIL with controlled RLT, which are depicted in Fig. 4(c) [116]. By using the PDMS dot array mold and dispensing module with a doctor blade, flexible microscale metastructures of dot arrays with various diameters were fabricated continuously.

Fabricating large-area and flexible molds for R2R NIL has been actively researched [117–121]. A flexible NIL mold with a hard PDMS (h-PDMS)/PDMS hybrid structure was fabricated for the UV R2R NIL system, as shown in Fig. 5(a) [122]. The hybrid stamp played roles as both a release agent transfer module and a lithographic template. The fabrication process of the mold follows that detailed by Odom et al. [123], but with modifications to the prepolymer formulation because the h-PDMS prepared according to the literature formulation is brittle. The generated h-PDMS obtained a bulk modulus of ~6 MPa, an approximately threefold increase on general PDMS, and significantly improved resistance to cracking at large area. Another method to fabricate flexible molds was introduced by using anodized aluminum oxide (AAO), as displayed in Fig. 5(b) [124]. The AAO/PDMS bi-layer mold was not damaged even after 180° bending due to the flexible PDMS. As a result, the mold was successfully employed to fabricate polymeric nanostructures through R2R NIL. Ni electroplating was also widely used to fabricate flexible and large-area molds because of its uniform and high-resolution replicating property even on the nanopatterned surface at macroscale [125–127]. A mechanical approach to manufacture the large-area and flexible mold was also studied using visually tolerable tilling (VTT), as shown in

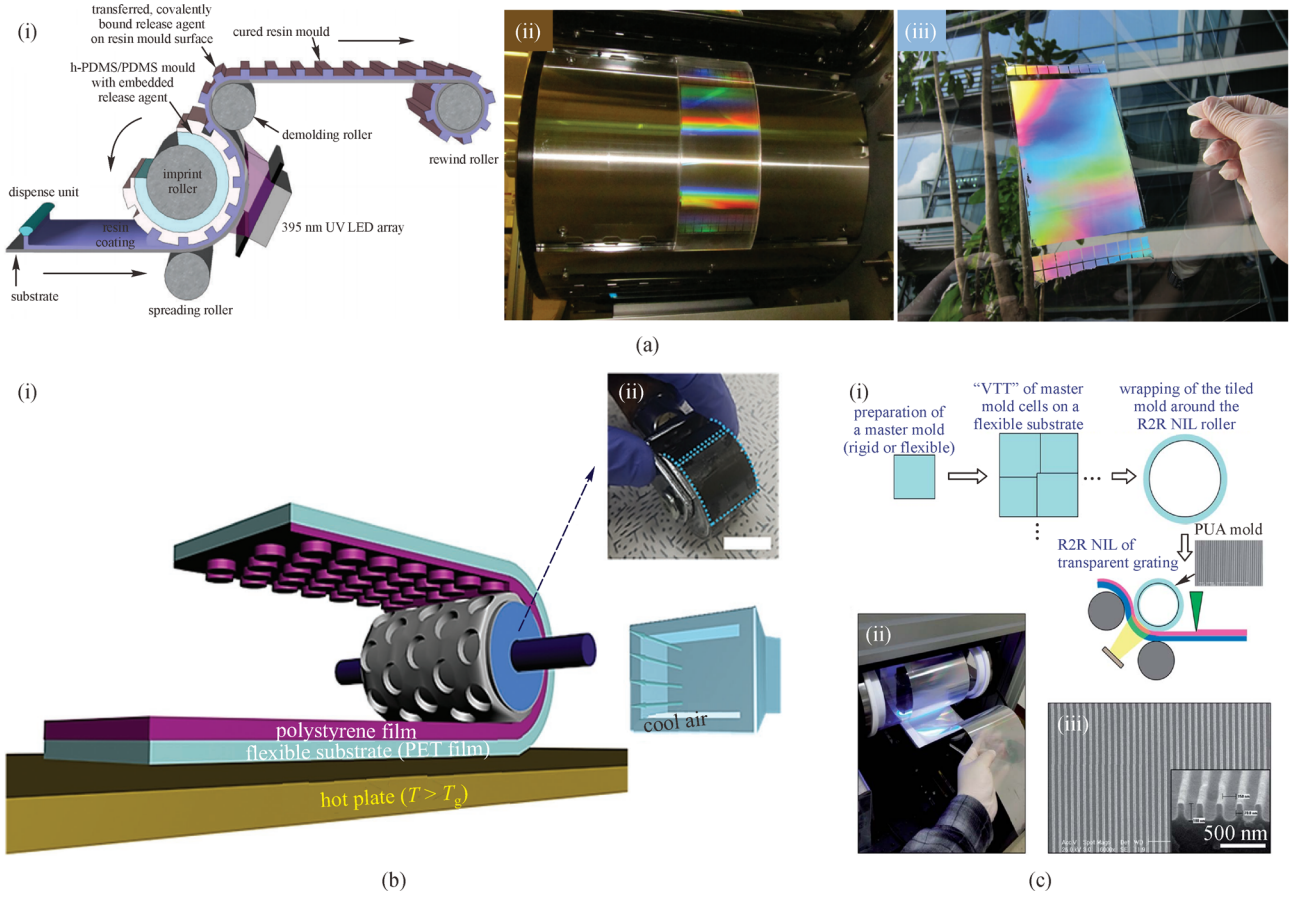

Fig. 5 Methods to fabricate large-area R2R NIL molds. (a) (i) Schematic of UV R2R NIL system, (ii) photographs of hard PDMS (h-PDMS)/PDMS composite stamps, and (iii) the corresponding nanopatterns fabricated via UV R2R NIL. Reprinted with permission from Ref. [122], Copyright 2016, The Royal Society of Chemistry. (b) (i) Schematic of R2R NIL to produce nanostructures on a polystyrene (PS) substrate and (ii) photograph of the roller attached by four hybrid molds with anodized aluminum oxide (AAO)/PDMS. Reprinted with permission from Ref. [124], Copyright 2018, John Wiley & Sons. (c) (i) Schematic of the R2R NIL process by tiling flexible molds, (ii) photograph of the R2R NIL using the large-area flexible mold, and (iii) SEM image of the fabricated nanostructures. Reprinted with permission from Ref. [128], Copyright 2015, The Royal Society of Chemistry

Fig. 5(c) [128]. This method enabled the large-area fabrication of seamless nanopattern molds by overlapping small stamps with nanopatterns composed of the dewetting and self-replicable resin under suitable pressure.

As an alternative, line-to-line (L2L) processes have been introduced to achieve limitless productivity [129,130]. L2L UV NIL was studied for the limitless fabrication of nanopatterns, called nanochannel-guided lithography (NCL), as depicted in Fig. 6(a) [131]. An SSQ resin on a polymer substrate was inscribed using the edge of a grating mold and then cured through UV light simultaneously, generating high-aspect-ratio nanopatterns continuously. The deformed plastic substrate by NCL delayed the collapse of the liquid nanopatterns, allowing time for the resin to be solid nanostructures. Because of the distinct lines of the resin, NCL was considered a residual layer-free process.

Contrary to NCL using a UV resin, L2L NIL process directly on polymer substrates, called dynamic nanoinscribing (DNI), was actively researched [132,133]. Using the unique property of the glass transition temperature (T_g), in which polymer substrates are made softer and are more easily deformed, nanopatterns were locally inscribed on the polymer substrate at T_g and as they are cooled rapidly, the nanostructures are solidified. In addition, through modulation of the process temperature, force, and speed of DNI, tailored nanopatterning was enabled continuously, as shown in Fig. 6(b) [134]. Additionally, vibrational indentation patterning (VIP) goes as far as to eliminate the heating source of DNI, fabricating nanopatterns using the only vibration of the mold, as seen in Fig. 6(c) [135]. In the VIP process, a rotational oscillation of the mold with eccentric mass caused to engrave periodic nanopatterns on the polymer substrate. By adjusting the angular speed, the harmonic function has different properties, making different depths, pitches, and shapes of nanopatterns. Although L2L NIL processes are still limited to produce nanopatterns with monotonous shapes such as gratings because of its simple mechanism, the mechanics enable L2L processes to be integrated with other conventional processes for the fabrication of multi-dimensional nanopatterns [136].

3.2 NIL for scalable fabrication of metasurfaces

Large-area and continuous fabrication of metasurfaces has been researched actively due to the development of scalable NIL [137]. Plasmonic metasurfaces with nanobumps were made largely using NIL, as demonstrated in Fig. 7(a) [138]. First, periodic nanopattern arrays on a

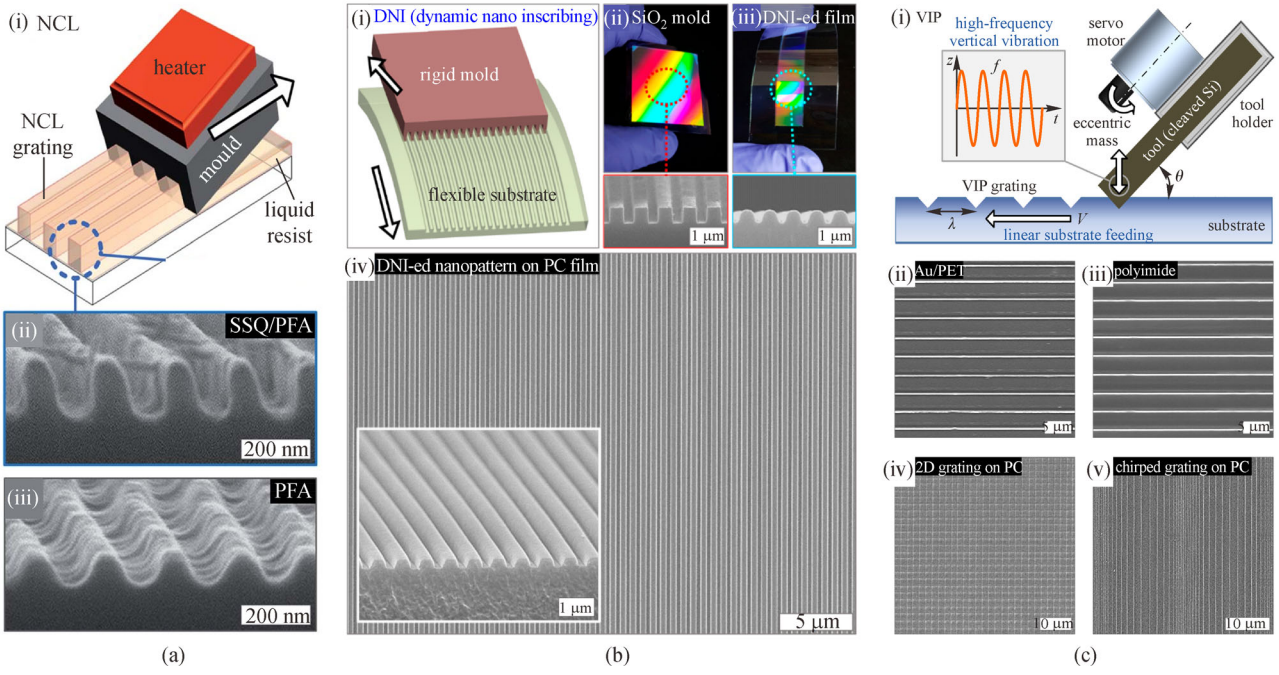

Fig. 6 Alternative NIL methods using local contact for high productivity. (a) (i) Schematic of the nanochannel-guided lithography (NCL) and SEM images of nanogratings with 200 nm period formed on the perfluoroalkoxy (PFA) substrates (ii) with and (iii) without a liquid SSQ resin. Reprinted with permission from Ref. [131], Copyright 2011, John Wiley & Sons. (b) (i) Schematic of dynamic nanoinscribing (DNI), photographs and SEM images of (ii) the rigid nanograting mold and (iii) the flexible substrate after DNI, and (iv) SEM images of nanopatterns fabricated by DNI. Inset to (iv) is an enlarged perspective view. Reprinted with permission from Ref. [134], Copyright 2019, American Chemical Society. (c) (i) Schematic of vibrational indentation patterning (VIP) with the process parameters and SEM images of grating patterns with 3 μm periods produced by VIP on (ii) 50 nm Au-coated PET and (iii) polyimide (PI). SEM images of (iv) two-dimensional (2D) nanopatterns of 2 μm period fabricated on polycarbonate (PC) and (v) nanostructures with various periods on PC fabricated by modulating the vibration frequency of VIP. Reprinted with permission from Ref. [135], Copyright 2013, John Wiley & Sons

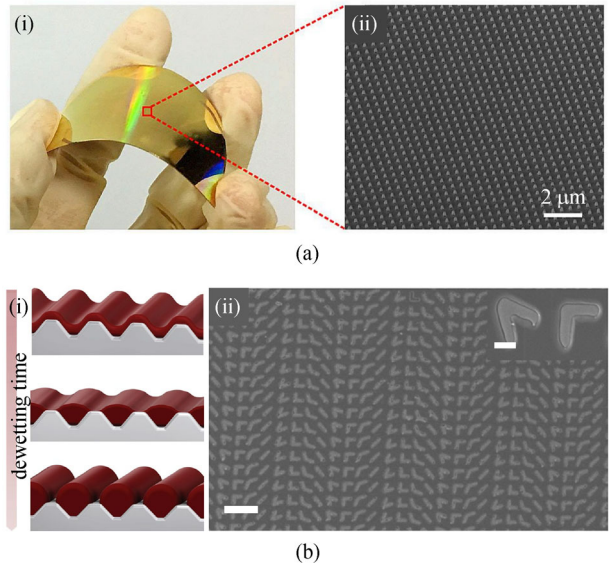

Fig. 7 Large-area fabrication of metasurfaces using conventional NIL. (a) (i) Photograph and (ii) SEM image of the large-area metasurface. Reprinted with permission from Ref. [138], Copyright 2020, Elsevier. (b) (i) Schematic of continuous line formation process and (ii) SEM image of the metasurface. Scale bars, 10 μm (large image) and 1 μm (inset). Reprinted with permission from Ref. [139], Copyright 2019, Nature Publishing Group

polycarbonate (PC) substrate were imprinted by thermal NIL. After that, the nanostructures were changed by oxygen plasma etching and then Au was deposited, fabricating uniform large-area metasurfaces. Soft NIL was also utilized easily for the fabrication of glass with large-area metasurfaces, as seen in Fig. 7(b) [139]. Soft NIL was first used to fabricate a PDMS mask onto a polymer substrate. And then, a chalcogenide glass film was deposited on the substrate by thermal evaporation or other approaches, before annealing was performed at different times and temperatures. This approach was both simple and scalable, where a 20 cm × 11 cm PC sheet with uniform nanostructures was imprinted, realizing state-of-the-art all-dielectric metasurfaces.

Going one step further, R2R NIL has been researched for the continuous fabrication of large-area metasurfaces in thermal and UV R2R NIL [140–143]. In the former, large-area nanostructures realizing structural coloring with surface plasmon resonance (SPR) were fabricated by thermal R2R NIL, as described in Fig. 8(a) [144]. The flexible patterned Ni mold was wrapped with a diameter of 66 mm roll. And then the roll heated by T_g of the target materials was pressed with a force of 600 N against a cold backing roll, resulting in a local force between the rolls of ≈ 1000 N. After deposition of aluminum (Al) layer, metasurfaces with structural colors by localized surface plasmon resonances (LSPRs) were produced continuously. Structural coloring metasurfaces were also fabricated by a high-speed thermal R2R NIL [145]. The nanostructured polypropylene (PP) with a constant depth of ~100 nm, various diameters, and pitch was produced by R2R NIL with a 45 cm wide web at a rate of 166.7 mm/s. Subsequently, the nanostructures were metalized to Al by the R2R thermal evaporation system. Consequently, owing to a coupling of cavity and pillar plasmon resonances, various structural colors were obtained in the visible spectrum.

Next, in the latter, scalable fabrication of flexible metasurface films was realized via UV R2R NIL and applied to broadband plasmonic infrared (IR) filters, as shown in Fig. 8(b) [146]. First, a UV curable SSQ resin was coated on a metal-insulator-metal (MIM) stack of Al (100 nm)/SiO_2 (200 nm)/Al (100 nm), and then UV R2R NIL was employed at the speed of 16.7 mm/s to produce nanopatterns continuously in the UV cured SSQ. Next, the nanopatterned SSQ was used as a mask to etch the top of Al layer of the MIM stack, fabricating a dual-band IR filtering array. In the IR filter, the reflection from neighboring narrow bands was overlapped and merged to form a broad reflection band. Furthermore, uniform plasmonic nanostructures were produced continuously by UV R2R NIL integrated with the conformal airbrushing process, as depicted in Fig. 8(c) [147]. After the PUA film was coated onto the flexible PET substrate by airbrushing, UV R2R NIL was performed on the PUA film by a flexible PDMS mold with the 100 nm-high and 200 nm-periodic nanopatterns. Subsequently, the 30 nm-thick Au film was thermally evaporated at three oblique angles (5°, 35°, and 50°) on the imprinted PUA nanogratings to make different nanostructures and induce other plasmonic phenomena, respectively. Consequently, large-area double-bent Au strips enabled to lengthen the oscillation path of surface plasmon, enhancing the sensitivity of refractive index about 210 nm/RIU. As a follow-up study, the double-bent Au strips were also applied to a plasmonic sensor showing size-dependent sensitivity [148].

As mentioned above, scalable NIL and its applications for large-area fabrication of metasurfaces have been actively studied. However, for NIL to be a genuine high-throughput process, NIL should easily produce customized nanopatterns for desired applications, which will be described in the next section.

4 NIL for complex nanopatterns and its practical fabrication of metasurfaces

To create tailored nanopatterns, NIL goes beyond being used by itself, it can be easily combined with other nanofabrication methods thanks to its mechanical embossing process [149–151]. In this section, actively controllable NIL methods for fabricating complex nanostructures will be discussed in detail. First, NIL for easy fabrication of hierarchical nanostructures will be described. Subsequently, to achieve higher resolution, NIL with modulating

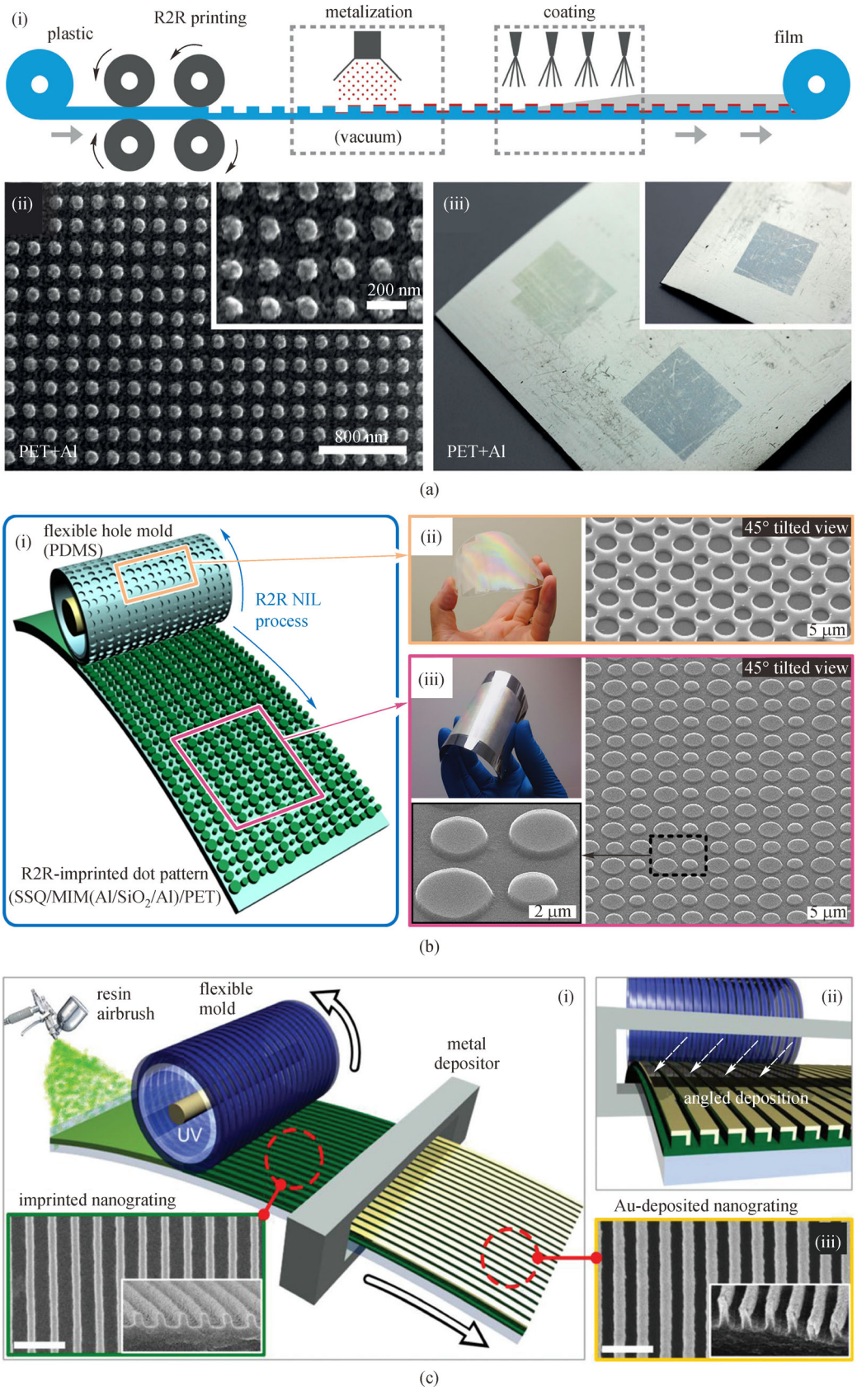

Fig. 8 Continuous fabrication of metasurfaces using R2R NIL. (a) (i) Schematic of anticipated R2R process, (ii) SEM images, and (iii) photographs of the imprinted amorphous polyethylene terephthalate (A-PET) polymer surface. Reprinted with permission from Ref. [144], Copyright 2016, John Wiley & Sons. (b) (i) Schematic of the R2R NIL process fabricating the metal-insulator-metal (MIM)-based metasurfaces and photographs and SEM images of (ii) large-area PDMS mold and (iii) SSQ dot patterns. Reprinted with permission from Ref. [146], Copyright 2012, American Institute of Physics. (c) (i) Schematic of continuous R2R NIL for fabricating plasmonic nanostructures, (ii) photograph and SEM image of angled Au evaporation, and (iii) SEM images after Au evaporation. Reprinted with permission from Ref. [147], Copyright 2017, The Royal Society of Chemistry

molds and resins will be discussed. At the end of this section, the practical fabrication of metasurfaces using NIL will be explained in detail.

4.1 NIL for actively modulating the morphology of nanopatterns

4.1.1 NIL for the fabrication of hierarchical nanostructures

Despite the perfect replication properties of NIL [152], the direct fabrication of the NIL molds with complex nanostructures through EBL is time-consuming and causes low productivity. To overcome these drawbacks, various NIL techniques were researched to enable lamination of nanostructures by modulating the properties of the NIL resins, as shown in Fig. 9(a) [153]. The UV-curable PUA resin was used for the fabrication of hierarchical nanohairs by 2-step UV-assisted capillary force lithography. After the PUA resin was partially cured using a PDMS mold with micropatterns by UV exposure, a mold with oblique nanopatterns was placed on the preformed micropatterns and subsequently cured by UV exposure, making the hierarchical structures. Another research used azobenzene which becomes a liquid at room temperature and directionally flows parallel to the light polarization under

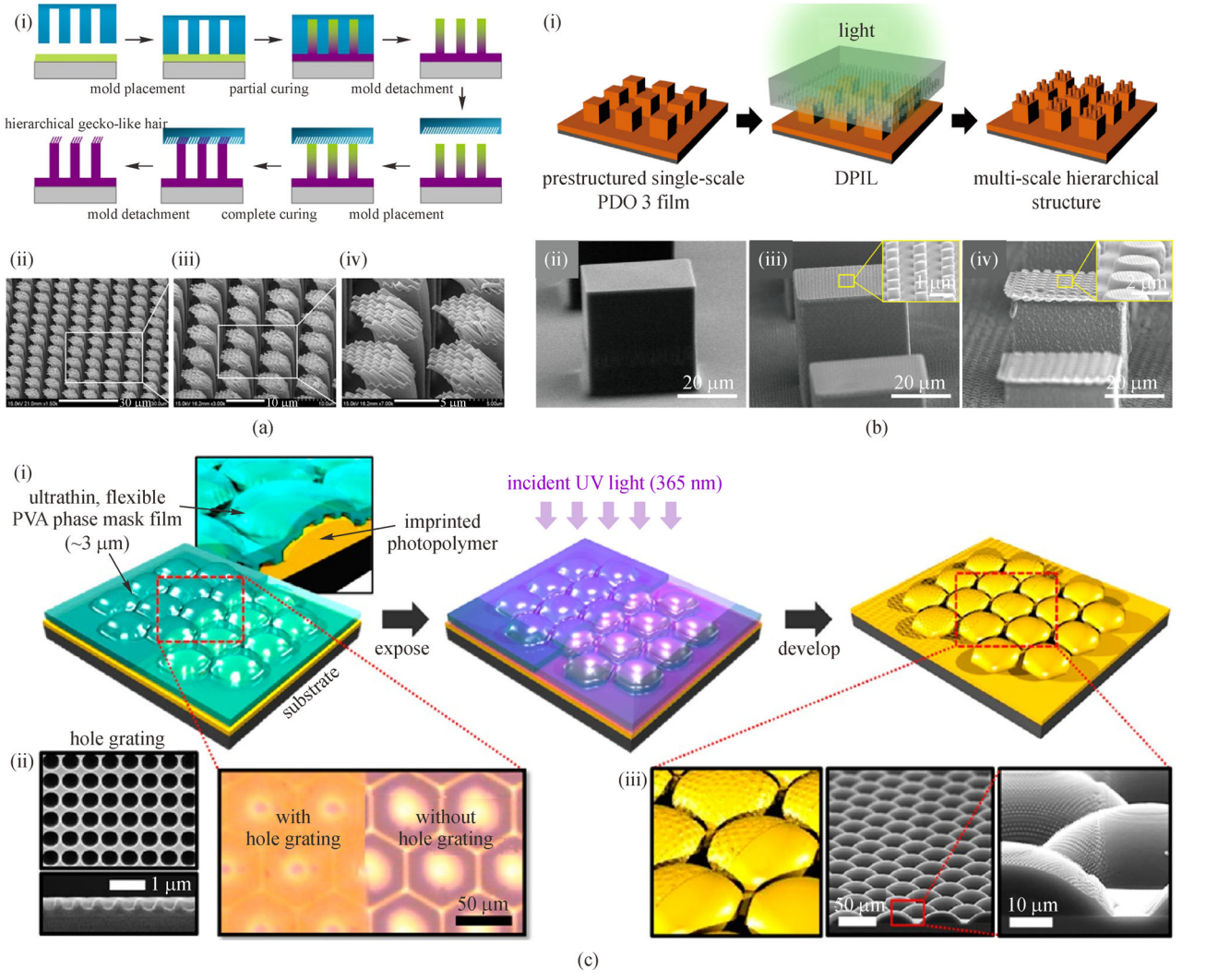

Fig. 9 NIL methodologies for fabrication of hierarchical nanostructures. (a) (i) Schematic of the fabrication of hierarchical nanohairs by 2-step UV-assisted capillary force lithography and (ii)–(iv) tilted SEM images of large-area hierarchical nanohairs. Reprinted with permission from Ref. [153], Copyright 2009, National Academy of Sciences. (b) (i) Schematic of the two-step light exposure process and SEM images of (ii) a micropattern, (iii) dual-scale structures, and (iv) triple-scale structures with a sub-100 nm size. Reprinted with permission from Ref. [155], Copyright 2017, American Chemical Society. (c) (i) Schematic describing flexible near-field phase-shift lithography (NFPSL) and photographs and SEM images of substrates (ii) before and (iii) after NFPSL. Reprinted with permission from Ref. [163], Copyright 2016, American Chemical Society

illumination [154]. Researchers applied the vertical movement of the azo driven by directional photofluidization, referring to it as directional photofluidization imprint lithography (DPIL), as demonstrated in Fig. 9(b) [155]. By controlling the optical penetration depth of azobenzene, it was allowed to selectively follow photofluidization at the surface, which enabled nanostructures to be fabricated on the top surface of the microstructures without deformation of the structures or structural collapsing. As a follow-up study, the researchers fabricated superomniphobic surfaces with mushroom-shaped micropillars by using the aforementioned properties of the azo-material [156].

NIL has also enabled to easily produce hierarchical nanostructures due to methods based on mechanical patterning [157–159]. Furthermore, soft NIL using flexible molds replicated the shape of the mold even on arbitrary substrates [160–162]. An ultrathin and flexible poly(vinyl alcohol) (PVA) phase mask film was used for the generation of hierarchical structures, as seen in Fig. 9(c) [163]. The hierarchical structures biologically inspired by insect eyes were fabricated through flexible phase masks enabling conformal contact even on arbitrary surfaces due to interaction of van der Walls force. Also, hierarchical micro-nano structures were produced even on a fragile substrate [164]. By integrating the flexible mold composed of PET/PDMS and the nanostructured UV-PDMS with the electric field, it was enabled for the mold to be contacted conformally with minimal stress on the fragile microconvex substrate. Additionally, the pressure of the process for manufacturing hierarchical micro-nano structures was controlled by changing the driven electric field easily.

4.1.2 NIL for fabrication of smaller nanopatterns

Besides facile fabrication of complex nanostructures, NIL also has been studied to fabricate smaller nanopatterns in terms of pre-processing and post-processing of NIL. The pre-processing has been mainly conducted by changing size of the mold [165,166]. A PDMS mold was fabricated by using single-walled carbon nanotubes (SWNTs) about 2 nm width as the original mold, as depicted in Fig. 10(a) [167]. After the transparent PDMS mold was fabricated with features of relief in the geometry of the SWNTs, a polyurethane (PU) resin was imprinted by the mold, enabling high resolution with a single-digit nanometer range. Carbon nanotubes (CNTs) were also used for etching mask to replicate the soft mold with small nanostructures [168]. The poly(methyl methacrylate) (PMMA) resin with CNTs was replicated by h-PDMS, forming nanoscale trenches that are inverse to the original lines of CNTs. Also, the chemical etching process was integrated with NIL to minimize size of the mold, as seen in Fig. 10(b) [169]. As 132, 189, and 240 s of etching time was applied at a steady rate of about 1.66 A/s, the linewidth of the SiO_2 nanopatterns on the NIL mold was shrunk from 50 to 33, 20, and 9.3 nm, respectively. Also, atomic layer deposition (ALD) process was applied on the NIL mold to generate tiny nanostructures, as displayed in Fig. 10(c) [170]. ALD of amorphous aluminum oxide (Al_2O_3) was conducted on both hard (at 225°C) and soft (at 100°C) molds, reducing the feature size of soft and hard molds to sub-5 nm.

Post-processing of NIL for smaller nanopatterns has been also researched mainly by modulating feature sizes of NIL resin [171,172]. A size modification of SSQ resin was conducted by a thermal reduction to fabricate sub-10 nm nanostructures, which is shown in Fig. 11(a) [173]. The SSQ resin was spin-coated on a silicon substrate and imprinted by UV NIL at room temperature within a few seconds to produce a first generation (1-G) template. And then the 1-G template was placed on a furnace or a hot plate for 1 h to produce a mold with reduced size. Furthermore, a linewidth of nanostructures was tuned by etching the residual layer of the imprinted resin, as seen in Fig. 11(b) [174]. Modulating etch rate caused sidewall smoothening as well as reduction of linewidths, which is of great significance for some photonic devices operating with a high-Q resonance such as guided-mode resonance (GMR) gratings since the optical performance of the device can be negatively affected by the line edge roughness [175].

In addition to aforementioned methods, various NIL studies for complex or small nanostructures have also been conducted by using alternative materials or by adjusting the mechanical properties of the resin [176,177]. In this way, NIL has tried to customize morphology of nanostructures actively in many ways. As a result, NIL has led diverse applications to control sizes or shapes of metasurfaces, which will be mentioned next.

4.2 Applications of NIL for practical fabricating metasurfaces

NIL has transferred shapes and sizes of nanostructures optionally, enabling flexible manufacturing system for fabrication of desired metasurfaces [178–182]. For instance, color filters with angle-insensitive structures realizing strong resonance in subwavelength gratings were fabricated by controlling the width of nanopatterns using NIL, as shown in Fig. 12(a) [183]. SiO_2 molds were imprinted thermally to create yellow, magenta, and cyan colors on a PMMA resin, respectively. After deposition of Cr and amorphous Si (a-Si) and lift-off process, vivid color filters with a-Si nanograting structures were finally fabricated. A switchable all-dielectric metasurface for full-color display was also produced by adjusting nanopattern parameters such as the pitch, width, TiO_2 height, and SiO_2 height using NIL [184]. Two resonant modes of the metasurface at proper positions realized the selectively

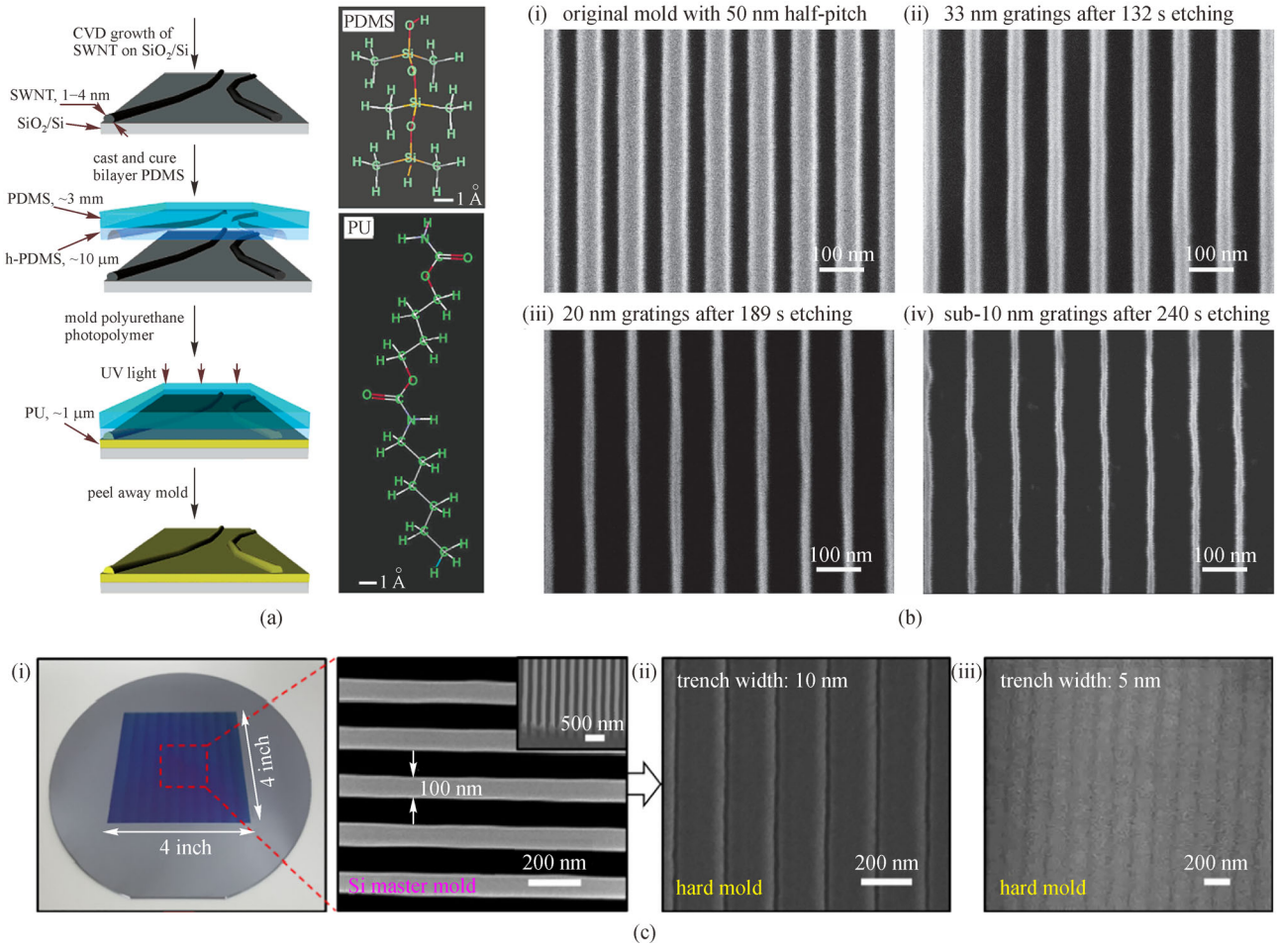

Fig. 10 Fabrication of NIL molds with smaller nanopatterns. (a) Steps for polymer imprint lithography with nanometer resolution and several repeat units of the PDMS and polyurethane (PU). Reprinted with permission from Ref. [167], Copyright 2004, American Chemical Society. (b) SEM images of (i) original SiO_2 master mold with 60 nm half-pitch, (ii) 33 nm wide nanowires (NWs) after etching for 132 s, (iii) 20 nm wide NWs after 189 s etching, and (iv) 9.3 nm wide NWs after 240 s etching. Reprinted with permission from Ref. [169], Copyright 2016, IOP Publishing. (c) (i) Photograph and SEM image of the mold with 200 nm-period nanogratings and SEM images of nanotrenches with widths of (ii) 10 nm and (iii) 5 nm in the hard mold after the atomic layer deposition (ALD) process. Reprinted with permission from Ref. [170], Copyright 2019, Elsevier

broad bandwidth (≈ 100 nm) and high efficiency (≈ 80%) in reflection. Furthermore, meta-mirrors have been fabricated by NIL, as seen in Fig. 12(b) [185]. First, the master mold manufactured by EBL and reactive ion etching (RIE) was replicated by UV NIL. Then, Ag deposition was applied to the replicated mold for the metasurface fabrication. The fabricated metasurface was transferred onto the organic light-emitting diode (OLED) substrate and capsulated, enabling a final meta-mirror with a pixel density of 10000 pixels per inch (PPI) in an red-green-blue-green arrangement and to 15000 PPI in a pentile-type arrangement.

By modulating the properties of the NIL resin, the properties of metasurfaces have also been changed [186]. As an example, TiO_2 nanoparticle was used as the NIL resin [187]. Dielectric metasurfaces having sub-100 nm resolution were fabricated using a TiO_2 particle-embedded UV-curable polymer resin (PER), as seen in Fig. 12(c) [188]. Variations in the refractive index of the PER is influenced by the TiO_2 nanoparticle concentration in the resin, allowing the direct fabrication of flexible metasurfaces using NIL without secondary processes such as deposition or etching processes. As a follow-up study, not only the refractive index but also the size of nanopatterns were adjusted simultaneously through the addition of TiO_2 nanoparticle, as shown in Fig. 12(d) [189]. Six kinds of nanoparticle composites (NPCs) from 0% to 100% of the TiO_2 weight ratio were spin-coated and imprinted. Accordingly, the refractive index was changed by using the Cauchy dispersion model at the same time, resulting in a plum pudding metalens (PPML) with a focusing efficiency of 33% at the target wavelength of 532 nm. Besides, gate-tunable and large-area graphene nanohole arrays (GNHAs) operating at mid-IR wavelengths were

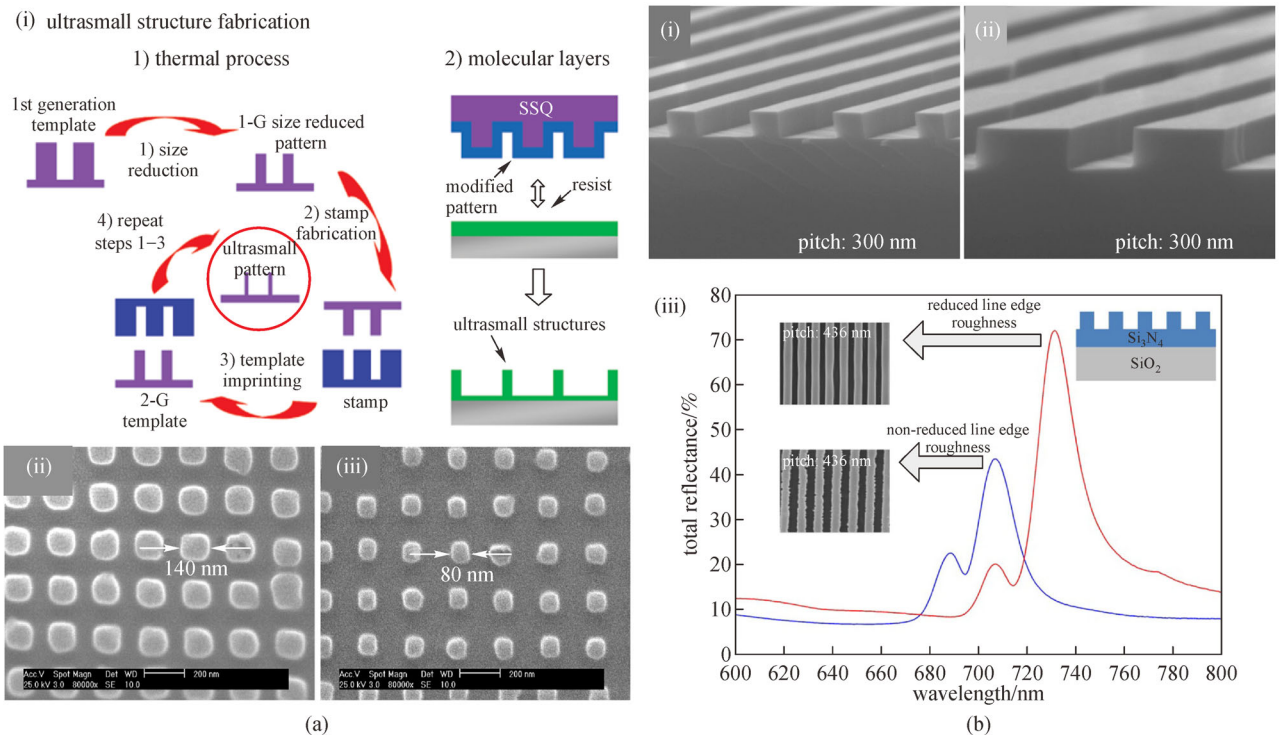

Fig. 11 Fabrication of nanopatterns with smaller sizes after NIL. (a) (i) Process flow for fabrication of ultrasmall structure with SSQ patterns and SEM images of (ii) nanopillar sample of 140 nm size and (iii) first generation (1-G) nanopatterns with 80 nm size after heated to 700°C. Reprinted with permission from Ref. [173], Copyright 2011, American Chemical Society. (b) SEM images of 1D grating with (i) low and (ii) high duty cycle of etching time and (iii) reflectance of guided-mode resonance (GMR) gratings fabricated with and without line edge roughness. Reprinted with permission from Ref. [174], Copyright 2015, Springer

studied for surface-enhanced infrared absorption (SEIRA) sensing [190]. By properly adjusting the geometrical parameters of the system through NIL, the position of exciting multiband plasmonic resonances was achieved.

Post-processing of NIL such as deposition also enabled a variety of tailored nanostructures to be straightforwardly engineered [191,192]. In particular, angled deposition of metals to imprinted nanopatterns has been actively researched because it produces complex metal nanostructures at once [147,148,193]. For instance, metasurfaces with polarization-dependent response were fabricated by NIL and oblique angle deposition (OAD) of Ag [194]. The imprinted nanostructures were placed on a customized evaporator enabling to control tilt angle θ, followed by oblique thermal evaporation of 75 nm of Ag. Three different tilt angles of Ag evaporation allowed to change geometrical parameters of each evaporated sample, causing a facile shift of resonances.

5 Conclusions and perspectives

To summarize, NIL is currently one of the most researched technologies in nanofabrication due to its facile accessibility and superior replicating property. Fabrication of metasurfaces using NIL opens new avenues because it can overcome the drawbacks of EBL such as small-area fabrication and the diffraction limit. Consequently, NIL provides possibilities for the high-throughput fabrication of promising metasurfaces. In this review, we focused on high-throughput NIL methods and their practical applications for the fabrication of metasurfaces.

First, conventional NIL composed of thermal NIL, UV NIL, and soft NIL was summarized to establish the classification of NIL. Subsequently, NIL with various materials such as metals, dielectrics, and other promising materials for the fabrication of metasurfaces was discussed. In particular, NIL can easily produce not only periodic but also aperiodic metasurfaces since the arbitrary nanopatterns are mechanically replicated regardless of the properties and morphologies.

Second, scalable NIL and its practical applications for large-area fabrication of metasurfaces were described. Beyond P2P NIL for the large-area fabrication of nanostructures, R2R NIL which can continuously fabricate nanopatterns realized the constant fabrication of nanopatterns. Although they had some challenges such as experimental errors, poor resin properties, and the absence of fabrication of large-area flexible mold, these drawbacks have been solved steadily. Moving forward, L2L NIL was introduced with unprecedented high productivity and facile application on various flexible substrates. Even if it

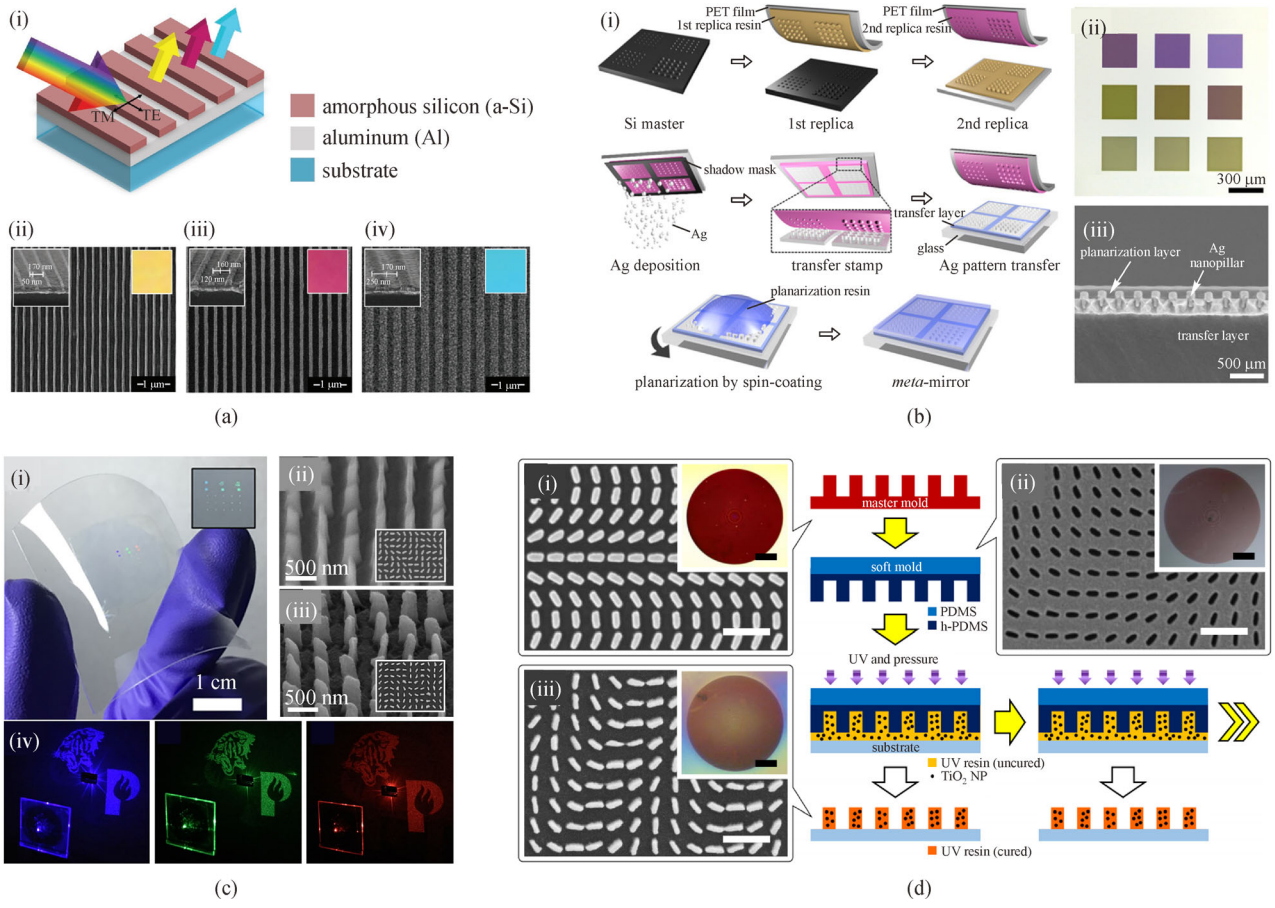

Fig. 12 Applications of NIL for high-throughput fabrication of metasurfaces. (a) (i) Schematic of the color filters with angle-insensitive structures and SEM images of fabricated (ii) yellow, (iii) magenta, and (iv) cyan color filters. Reprinted with permission from Ref. [183], Copyright 2016, John Wiley & Sons. (b) (i) Schematic of meta-mirror fabrication, (ii) optical microscope images of nine meta-mirrors with the size of 300 μm × 300 μm, and (iii) SEM image of the fabricated silver (Ag) meta-mirrors. Reprinted with permission from Ref. [185], Copyright 2020, American Association for the Advancement of Science. (c) (i) Photograph of the metasurface on the flexible substrate, SEM images of (ii) the master mold and (iii) the transferred metasurface on a glass substrate, and (iv) hologram images of the optimized metasurface by radiating lasers of λ = 450, 532, and 635 nm, respectively. Reprinted with permission from Ref. [188], Copyright 2019, American Chemical Society. (d) Fabrication schematic of plum pudding metalens using nanoparticle composite NIL and SEM images of (i) master mold, (ii) soft mold, and (iii) final metasurfaces, respectively. All scale bars: 1 μm. (Insets) Optical microscope images of each. All scale bars: 100 μm. Reprinted with permission from Ref. [189], Copyright 2020, Nature Publishing Group

still has limitations for the fabrication of nanopatterns with simple shapes, its extraordinary nanofabrication speed is well worth continuing research. Furthermore, scalable fabrication of metasurfaces through NIL was summarized. Especially, plasmonic color metasurfaces were fabricated by thermal R2R NIL even at a rate of 166.7 mm/s, realizing NIL as the next-generation process for large-area metasurfaces.

Third, flexible NIL techniques for the fabrication of tailored nanopatterns and its applications for metasurfaces were introduced. Complex nanopatterns such as hierarchical structures were fabricated by modulating NIL resin properties or using flexible molds. Azobenzene, for example, was applied as directional photofluidization imprint lithography, fabricating hierarchical structures straightforwardly. Moreover, NIL with high resolution was achieved by integrating with conventional nanofabrication methods. Representatively, thermal annealing was mainly used to fabricate sub-10 nm nanostructures, showing the potential of NIL for single-digit resolution. Finally, NIL integrated with conventional deposition processes for fabricating metasurfaces was discussed. Among them, OAD has been actively applied to imprinted nanostructures, easily modulating optical properties of metasurfaces.

NIL is emerging as a prospective fabrication method because it aims to achieve both high productivity and high resolution, which are difficult to be attained in existing nanofabrication methods. Furthermore, NIL can be applied to produce large-area and high-resolution metasurfaces by itself or by the integration with other conventional nanofabrication processes. Beyond this great prospect,

NIL is worthy to be developed in specific directions. First, continuous NIL has attained high productivity but is still limited to the replication of monotonous shapes. So, convergence with a variety of nanofabrication techniques and promising materials to realize high-efficiency complex metasurfaces might be one of the main promising approaches going forward [195–199]. Next, NIL for the fabrication of tailored nanostructures has been already achieved but its practical applications for multifunctional metasurfaces are insufficient. Thus, the micromechanical analysis of NIL is also by no means exhaustive for the precise fabrication of metasurfaces, ultimately accelerating the development of active metasurfaces [200–202].

Acknowledgements This work was financially supported by the National Research Foundation (NRF) grant (NRF-2019R1A2C3003129) funded by the Ministry of Science and ICT, Republic of Korea. T.L. acknowledges the NRF Global Ph.D. fellowship (NRF-2019H1A2A1076295) funded by the Ministry of Education, Republic of Korea.

References

1. Lemoult F, Kaina N, Fink M, Lerosey G. Wave propagation control at the deep subwavelength scale in metamaterials. Nature Physics, 2013, 9(11): 55–60
2. Lee C W, Choi H J, Jeong H. Tunable metasurfaces for visible and SWIR applications. Nano Convergence, 2020, 7(1): 3
3. Chen Y, Ai B, Wong Z J. Soft optical metamaterials. Nano Convergence, 2020, 7(1): 18
4. Lawrence M, Barton D R 3rd, Dixon J, Song J H, van de Groep J, Brongersma M L, Dionne J A. High quality factor phase gradient metasurfaces. Nature Nanotechnology, 2020, 15(11): 956–961
5. Yoon G, Lee D, Nam K T, Rho J. Geometric metasurface enabling polarization independent beam splitting. Scientific Reports, 2018, 8(1): 9468
6. Wu P C, Pala R A, Kafaie Shirmanesh G, Cheng W H, Sokhoyan R, Grajower M, Alam M Z, Lee D, Atwater H A. Dynamic beam steering with all-dielectric electro-optic III-V multiple-quantum-well metasurfaces. Nature Communications, 2019, 10(1): 3654
7. Wong Z J, Wang Y, O'Brien K, Rho J, Yin X B, Zhang S, Fang N, Yen T J, Zhang X. Optical and acoustic metamaterials: Superlens, negative refractive index and invisibility cloak. Journal of Optics, 2017, 19(8): 084007
8. Bang S, So S, Rho J. Realization of broadband negative refraction in visible range using vertically stacked hyperbolic metamaterials. Scientific Reports, 2019, 9(1): 14093
9. Yu N, Capasso F. Flat optics with designer metasurfaces. Nature Materials, 2014, 13(2): 139–150
10. Lee D, Yang Y, Yoon G, Kim M, Rho J. Resolution enhancement of fluorescence microscopy using encoded patterns from all-dielectric metasurfaces. Applied Physics Letters, 2019, 115(10): 101102
11. Lee D, Kim M, Kim J, Hong H, Badloe T, Kim D S, Rho J. All-dielectric metasurface imaging platform applicable to laser scanning microscopy with enhanced axial resolution and wavelength selection. Optical Materials Express, 2019, 9(8): 3248–3259
12. Kim M, Rho J. Metamaterials and imaging. Nano Convergence, 2015, 2(1): 22
13. Byun M, Lee D, Kim M, Kim Y, Kim K, Ok J G, Rho J, Lee H. Demonstration of nanoimprinted hyperlens array for high-throughput sub-diffraction imaging. Scientific Reports, 2017, 7 (1): 46314
14. Lee D, Kim Y D, Kim M, So S, Choi H J, Mun J, Nguyen D M, Badloe T, Ok J G, Kim K, Lee H, Rho J. Realization of wafer-scale hyperlens device for sub-diffractional biomolecular imaging. ACS Photonics, 2018, 5(7): 2549–2554
15. Jang J, Badloe T, Yang Y, Lee T, Mun J, Rho J. Spectral modulation through the hybridization of Mie-scatterers and quasi-guided mode resonances: realizing full and gradients of structural color. ACS Nano, 2020, 14(11): 15317–15326
16. Mudachathi R, Tanaka T. Up scalable full colour plasmonic pixels with controllable hue, brightness and saturation. Scientific Reports, 2017, 7(1): 1199
17. Lee Y, Park M K, Kim S, Shin J H, Moon C, Hwang J Y, Choi J C, Park H, Kim H R, Jang J E. Electrical broad tuning of plasmonic color filter employing an asymmetric-lattice nanohole array of metasurface controlled by polarization rotator. ACS Photonics, 2017, 4(8): 1954–1966
18. Lee D, Gwak J, Badloe T, Palomba S, Rho J. Metasurfaces-based imaging and applications: from miniaturized optical components to functional imaging platforms. Nanoscale Advances, 2020, 2(2): 605–625
19. Lee T, Jang J, Jeong H, Rho J. Plasmonic- and dielectric-based structural coloring: from fundamentals to practical applications. Nano Convergence, 2018, 5(1): 1
20. Kim M, Kim I, Jang J, Lee D, Nam K T, Rho J. Active color control in a metasurface by polarization rotation. Applied Sciences (Basel, Switzerland), 2018, 8(6): 982
21. Yoon G, Lee D, Nam K T, Rho J. "Crypto-display" in dual-mode metasurfaces by simultaneous control of phase and spectral responses. ACS Nano, 2018, 12(7): 6421–6428
22. Jang J, Kang K, Raeis-Hosseini N, Ismukhanova A, Jeong H, Jung C, Kim B, Lee J Y, Park I, Rho J. Self-powered humidity sensor using chitosan-based plasmonic metal-hydrogel-metal filters. Advanced Optical Materials, 2020, 8(9): 1901932
23. Aoni R A, Rahmani M, Xu L, Zangeneh Kamali K, Komar A, Yan J, Neshev D, Miroshnichenko A E. High-efficiency visible light manipulation using dielectric metasurfaces. Scientific Reports, 2019, 9(1): 6510
24. Jang J, Badloe T, Sim Y C, Yang Y, Mun J, Lee T, Cho Y H, Rho J. Full and gradient structural colouration by lattice amplified gallium nitride Mie-resonators. Nanoscale, 2020, 12(41): 21392–21400
25. Kim I, Ansari M A, Mehmood M Q, Kim W S, Jang J, Zubair M, Kim Y K, Rho J. Stimuli-responsive dynamic metaholographic displays with designer liquid crystal modulators. Advanced Materials, 2020, 32(50): e2004664
26. Kim I, Yoon G, Jang J, Genevet P, Nam K T, Rho J. Outfitting next generation displays with optical metasurfaces. ACS Photonics, 2018, 5(10): 3876–3895
27. Li Z, Kim I, Zhang L, Mehmood M Q, Anwar M S, Saleem M, Lee D, Nam K T, Zhang S, Luk'yanchuk B, Wang Y, Zheng G, Rho J, Qiu C W. Dielectric meta-holograms enabled with dual magnetic

resonances in visible light. ACS Nano, 2017, 11(9): 9382–9389
28. Lee G Y, Yoon G, Lee S Y, Yun H, Cho J, Lee K, Kim H, Rho J, Lee B. Complete amplitude and phase control of light using broadband holographic metasurfaces. Nanoscale, 2018, 10(9): 4237–4245
29. Ansari M A, Kim I, Lee D, Waseem M H, Zubair M, Mahmood N, Badloe T, Yerci S, Tauqeer T, Mehmood M Q, Rho J. A spin-encoded all-dielectric metahologram for visible light. Laser & Photonics Reviews, 2019, 13(5): 1900065
30. Yoon G, Kim J, Mun J, Lee D, Nam K T, Rho J. Wavelength-decoupled geometric metasurfaces by arbitrary dispersion control. Communications on Physics, 2019, 2(1): 129
31. Ansari M A, Kim I, Rukhlenko I D, Zubair M, Yerci S, Tauqeer T, Mehmood M Q, Rho J. Engineering spin and antiferromagnetic resonances to realize an efficient direction-multiplexed visible meta-hologram. Nanoscale Horizons, 2020, 5(1): 57–64
32. Yoon G, Lee D, Nam K T, Rho J. Pragmatic metasurface hologram at visible wavelength: the balance between diffraction efficiency and fabrication compatibility. ACS Photonics, 2018, 5(5): 1643–1647
33. Ren H, Fang X, Jang J, Bürger J, Rho J, Maier S A. Complex-amplitude metasurface-based orbital angular momentum holography in momentum space. Nature Nanotechnology, 2020, 15(11): 948–955
34. Rana A S, Mehmood M Q, Jeong H, Kim I, Rho J. Tungsten-based ultrathin absorber for visible regime. Scientific Reports, 2018, 8(1): 2443
35. Barho F B, Gonzalez-Posada F, Cerutti L, Taliercio T. Heavily doped semiconductor metamaterials for mid-infrared multispectral perfect absorption and thermal emission. Advanced Optical Materials, 2020, 8(6): 1901502
36. Yoon G, So S, Kim M, Mun J, Ma R, Rho J. Electrically tunable metasurface perfect absorber for infrared frequencies. Nano Convergence, 2017, 4(1): 36
37. Nguyen D M, Lee D, Rho J. Control of light absorbance using plasmonic grating based perfect absorber at visible and near-infrared wavelengths. Scientific Reports, 2017, 7(1): 2611
38. Badloe T, Mun J, Rho J. Metasurfaces-based absorption and reflection control: perfect absorbers and reflectors. Journal of Nanomaterials, 2017, 2017(1): 2361042
39. Badloe T, Kim I, Rho J. Moth-eye shaped on-demand broadband and switchable perfect absorbers based on vanadium dioxide. Scientific Reports, 2020, 10(1): 4522
40. Badloe T, Kim I, Rho J. Biomimetic ultra-broadband perfect absorbers optimised with reinforcement learning. Physical Chemistry Chemical Physics, 2020, 22(4): 2337–2342
41. Kim I, So S, Rana A S, Mehmood M Q, Rho J. Thermally robust ring-shaped chromium perfect absorber of visible light. Nanophotonics, 2018, 7(11): 1827–1833
42. Sajedian I, Badloe T, Lee H, Rho J. Deep *Q*-network to produce polarization-independent perfect solar absorbers: a statistical report. Nano Convergence, 2020, 7(1): 26
43. Yoon G, Jang J, Mun J, Nam K T, Rho J. Metasurface zone plate for light manipulation in vectorial regime. Communications on Physics, 2019, 2(1): 156
44. Yin X, Ye Z, Rho J, Wang Y, Zhang X. Photonic spin Hall effect at metasurfaces. Science, 2013, 339(6126): 1405–1407
45. Wang Y H, Jin R C, Li J Q, Zhong F, Liu H, Kim I, Jo Y, Rho J, Dong Z G. Photonic spin hall effect by the spin-orbit interaction in a metasurface with elliptical nano-structures. Applied Physics Letters, 2017, 110(10): 101908
46. Wang Y H, Kim I, Jin R C, Jeong H, Li J Q, Dong Z G, Rho J. Experimental verification of asymmetric transmission in continuous omega-shaped metamaterials. RSC Advances, 2018, 8(67): 38556–38561
47. Hong J, Kim S J, Kim I, Yun H, Mun S E, Rho J, Lee B. Plasmonic metasurface cavity for simultaneous enhancement of optical electric and magnetic fields in deep subwavelength volume. Optics Express, 2018, 26(10): 13340–13348
48. Kim I, So S, Mun J, Lee K H, Lee J H, Lee T, Rho J. Optical characterizations and thermal analyses of HfO_2/SiO_2 multilayered diffraction gratings for high-power continuous wave laser. Journal of Physics: Photonics, 2020, 2(2): 025004
49. Mahmood N, Kim I, Mehmood M Q, Jeong H, Akbar A, Lee D, Saleem M, Zubair M, Anwar M S, Tahir F A, Rho J. Polarisation insensitive multifunctional metasurfaces based on all-dielectric nanowaveguides. Nanoscale, 2018, 10(38): 18323–18330
50. Mahmood N, Jeong H, Kim I, Mehmood M Q, Zubair M, Akbar A, Saleem M, Anwar M S, Tahir F A, Rho J. Twisted non-diffracting beams through all dielectric meta-axicons. Nanoscale, 2019, 11 (43): 20571–20578
51. Li Z, Dai Q, Mehmood M Q, Hu G, Yanchuk B L, Tao J, Hao C, Kim I, Jeong H, Zheng G, Yu S, Alù A, Rho J, Qiu C W. Full-space cloud of random points with a scrambling metasurface. Light, Science & Applications, 2018, 7(1): 63
52. Yoon G, Lee D, Rho J. Demonstration of equal-intensity beam generation by dielectric metasurfaces. Journal of Visualized Experiments, 2019, 148(148): e59066
53. Lee H E, Ahn H Y, Mun J, Lee Y Y, Kim M, Cho N H, Chang K, Kim W S, Rho J, Nam K T. Amino-acid- and peptide-directed synthesis of chiral plasmonic gold nanoparticles. Nature, 2018, 556 (7701): 360–365
54. Raeis-Hosseini N, Rho J. Dual-functional nanoscale devices using phase-change materials: a reconfigurable perfect absorber with nonvolatile resistance-change memory characteristics. Applied Sciences (Basel, Switzerland), 2019, 9(3): 564
55. Raeis-Hosseini N, Rho J. Metasurfaces based on phase-change material as a reconfigurable platform for multifunctional devices. Materials (Basel), 2017, 10(9): 1046
56. Yoon G, Kim I, So S, Mun J, Kim M, Rho J. Fabrication of three-dimensional suspended, interlayered and hierarchical nanostructures by accuracy-improved electron beam lithography overlay. Scientific Reports, 2017, 7(1): 6668
57. Seo I C, Woo B H, An S C, Lee E, Jeong H Y, Lim Y, Jun Y C. Electron-beam-induced nanopatterning of J-aggregate thin films for excitonic and photonic response control. Advanced Optical Materials, 2018, 6(20): 1800583
58. Jung C, Yang Y, Jang J, Badloe T, Lee T, Mun J, Moon S W, Rho J. Near-zero reflection of all-dielectric structural coloration enabling polarization-sensitive optical encryption with enhanced switchability. Nanophotonics, 2020, 10(2): 919–926
59. Zhou J, Qian H, Chen C F, Zhao J, Li G, Wu Q, Luo H, Wen S, Liu

Z. Optical edge detection based on high-efficiency dielectric metasurface. Proceedings of the National Academy of Sciences of the United States of America, 2019, 116(23): 11137–11140

60. Jeon T, Kim D H, Park S G. Holographic fabrication of 3D nanostructures. Advanced Materials Interfaces, 2018, 5(18): 1800330
61. Oh Y, Lim J W, Kim J G, Wang H, Kang B H, Park Y W, Kim H, Jang Y J, Kim J, Kim D H, Ju B K. Plasmonic periodic nanodot arrays via laser interference lithography for organic photovoltaic cells with $>10\%$ efficiency. ACS Nano, 2016, 10(11): 10143–10151
62. Bagheri S, Strohfeldt N, Sterl F, Berrier A, Tittl A, Giessen H. Large-area low-cost plasmonic perfect absorber chemical sensor fabricated by laser interference lithography. ACS Sensors, 2016, 1 (9): 1148–1154
63. Do Y S. A highly reproducible fabrication process for large-area plasmonic filters for optical applications. IEEE Access: Practical Innovations, Open Solutions, 2018, 6(1): 68961–68967
64. Song M, Li X, Pu M, Guo Y, Liu K, Yu H, Ma X, Luo X. Color display and encryption with a plasmonic polarizing metamirror. Nanophotonics, 2018, 7(1): 323–331
65. Gan Z, Cai J, Liang C, Chen L, Min S, Cheng X, Cui D, Li W D. Patterning of high-aspect-ratio nanogratings using phase-locked two-beam fiber-optic interference lithography. Journal of Vacuum Science & Technology B, Microelectronics and Nanometer Structures, 2019, 37(6): 060601
66. Liang G, Wang C, Zhao Z, Wang Y, Yao N, Gao P, Luo Y, Gao G, Zhao Q, Luo X. Squeezing bulk plasmon polaritons through hyperbolic metamaterials for large area deep subwavelength interference lithography. Advanced Optical Materials, 2015, 3(9): 1248–1256
67. Liu H C, Kong W J, Zhu Q G, Zheng Y, Shen K S, Zhang J, Lu H. Plasmonic interference lithography by coupling the bulk plasmon polariton mode and the waveguide mode. Journal of Physics D, Applied Physics, 2020, 53(13): 135103
68. Gao P, Pu M, Ma X, Li X, Guo Y, Wang C, Zhao Z, Luo X. Plasmonic lithography for the fabrication of surface nanostructures with a feature size down to 9 nm. Nanoscale, 2020, 12(4): 2415–2421
69. Luo J, Zeng B, Wang C, Gao P, Liu K, Pu M, Jin J, Zhao Z, Li X, Yu H, Luo X. Fabrication of anisotropically arrayed nano-slots metasurfaces using reflective plasmonic lithography. Nanoscale, 2015, 7(44): 18805–18812
70. Wang C, Zhang W, Zhao Z, Wang Y, Gao P, Luo Y, Luo X. Plasmonic structures, materials and lenses for optical lithography beyond the diffraction limit: A review. Micromachines, 2016, 7(7): 118
71. Kim S K. Impact of plasmonic parameters on 7-nm patterning in plasmonic computational lithography. Journal of Nanoscience and Nanotechnology, 2018, 18(10): 7124–7127
72. Hong F, Blaikie R. Plasmonic lithography: recent progress. Advanced Optical Materials, 2019, 7(14): 1801653
73. Kim I, Mun J, Baek K M, Kim M, Hao C, Qiu C W, Jung Y S, Rho J. Cascade domino lithography for extreme photon squeezing. Materials Today, 2020, 39(1): 89–97
74. Kim I, Mun J, Hwang W, Yang Y, Rho J. Capillary-force-induced collapse lithography for controlled plasmonic nanogap structures. Microsystems & Nanoengineering, 2020, 6(1): 65
75. Nam V B, Giang T T, Koo S, Rho J, Lee D. Laser digital patterning of conductive electrodes using metal oxide nanomaterials. Nano Convergence, 2020, 7(1): 23
76. Chou S Y, Krauss P R, Renstrom P J. Nanoimprint lithography. Journal of Vacuum Science & Technology B, Microelectronics and Nanometer Structures: Processing, Measurement, and Phenomena, 1996, 14(6): 4129–4133
77. Chou S Y, Krauss P R, Renstrom P J. Imprint lithography with 25-nanometer resolution. Science, 1996, 272(5258): 85–87
78. Chou S Y. Sub-10 nm imprint lithography and applications. Journal of Vacuum Science & Technology B, Microelectronics and Nanometer Structures: Processing, Measurement, and Phenomena, 1997, 15(6): 2897–2904
79. Haisma J, Verheijen M, van den Heuvel K, van den Berg J. Mold-assisted nanolithography: a process for reliable pattern replication. Journal of Vacuum Science & Technology B, Microelectronics and Nanometer Structures: Processing, Measurement, and Phenomena, 1996, 14(6): 4124–4128
80. Austin M D, Ge H, Wu W, Li M, Yu Z, Wasserman D, Lyon S A, Chou S Y. Fabrication of 5 nm linewidth and 14 nm pitch features by nanoimprint lithography. Applied Physics Letters, 2004, 84 (26): 5299–5301
81. Plachetka U, Bender M, Fuchs A, Vratzov B, Glinsner T, Lindner F, Kurz H. Wafer scale patterning by soft UV-nanoimprint lithography. Microelectronic Engineering, 2004, 73–74(1): 167–171
82. Sreenivasan S V. Nanoimprint lithography steppers for volume fabrication of leading-edge semiconductor integrated circuits. Microsystems & Nanoengineering, 2017, 3(1): 17075
83. Qiao W, Huang W, Liu Y, Li X, Chen L S, Tang J X. Toward scalable flexible nanomanufacturing for photonic structures and devices. Advanced Materials, 2016, 28(47): 10353–10380
84. Traub M C, Longsine W, Truskett V N. Advances in nanoimprint lithography. Annual Review of Chemical and Biomolecular Engineering, 2016, 7(1): 583–604
85. Kim M, Lee D, Kim T H, Yang Y, Park H J, Rho J. Observation of enhanced optical spin hall effect in a vertical hyperbolic metamaterial. ACS Photonics, 2019, 6(10): 2530–2536
86. Atighilorestani M, Jiang H, Kaminska B. Electrochromic-polymer-based switchable plasmonic color devices using surface-relief nanostructure pixels. Advanced Optical Materials, 2018, 6(23): 1801179
87. Lee D, Han S Y, Jeong Y, Nguyen D M, Yoon G, Mun J, Chae J, Lee J H, Ok J G, Jung G Y, Park H J, Kim K, Rho J. Polarization-sensitive tunable absorber in visible and near-infrared regimes. Scientific Reports, 2018, 8(1): 12393
88. Zhang H, Kinnear C, Mulvaney P. Fabrication of single-nanocrystal arrays. Advanced Materials, 2020, 32(18): e1904551
89. Yoon G, Kim I, Rho J. Challenges in fabrication towards realization of practical metamaterials. Microelectronic Engineering, 2016, 163(1): 7–20
90. Yao Y, Liu H, Wang Y, Li Y, Song B, Wang R P, Povinelli M L, Wu W. Nanoimprint-defined, large-area meta-surfaces for unidirectional optical transmission with superior extinction in the visible-

to-infrared range. Optics Express, 2016, 24(14): 15362–15372
91. Lee G Y, Hong J Y, Hwang S, Moon S, Kang H, Jeon S, Kim H, Jeong J H, Lee B. Metasurface eyepiece for augmented reality. Nature Communications, 2018, 9(1): 4562
92. Wan Y H, Krueger N A, Ocier C R, Su P, Braun P V, Cunningham B T. Resonant mode engineering of photonic crystal sensors clad with ultralow refractive index porous silicon dioxide. Advanced Optical Materials, 2017, 5(21): 1700605
93. Sutherland B R, Sargent E H. Perovskite photonic sources. Nature Photonics, 2016, 10(5): 295–302
94. Chun D H, Choi Y J, In Y, Nam J K, Choi Y J, Yun S, Kim W, Choi D, Kim D, Shin H, Cho J H, Park J H. Halide perovskite nanopillar photodetector. ACS Nano, 2018, 12(8): 8564–8571
95. Pourdavoud N, Wang S, Mayer A, Hu T, Chen Y, Marianovich A, Kowalsky W, Heiderhoff R, Scheer H C, Riedl T. Photonic nanostructures patterned by thermal nanoimprint directly into organo-metal halide perovskites. Advanced Materials, 2017, 29 (12): 1605003
96. Mao J, Sha W E I, Zhang H, Ren X G, Zhuang J Q, Roy V A L, Wong K S, Choy W C H. Novel direct nanopatterning approach to fabricate periodically nanostructured perovskite for optoelectronic applications. Advanced Functional Materials, 2017, 27(10): 1606525
97. Makarov S V, Milichko V, Ushakova E V, Omelyanovich M, Pasaran A C, Haroldson R, Balachandran B, Wang H L, Hu W, Kivshar Y S, Zakhidov A A. Multifold emission enhancement in nanoimprinted hybrid perovskite metasurfaces. ACS Photonics, 2017, 4(4): 728–735
98. Wang H, Liu S C, Balachandran B, Moon J, Haroldson R, Li Z, Ishteev A, Gu Q, Zhou W, Zakhidov A, Hu W. Nanoimprinted perovskite metasurface for enhanced photoluminescence. Optics Express, 2017, 25(24): A1162–A1171
99. Baek S W, Molet P, Choi M J, Biondi M, Ouellette O, Fan J, Hoogland S, García de Arquer F P, Mihi A, Sargent E H. Nanostructured back reflectors for efficient colloidal quantum-dot infrared optoelectronics. Advanced Materials, 2019, 31(33): e1901745
100. Kim Y, Bicanic K, Tan H, Ouellette O, Sutherland B R, García de Arquer F P, Jo J W, Liu M, Sun B, Liu M, Hoogland S, Sargent E H. Nanoimprint-transfer-patterned solids enhance light absorption in colloidal quantum dot solar cells. Nano Letters, 2017, 17(4): 2349–2353
101. Pina-Hernandez C, Koshelev A, Dhuey S, Sassolini S, Sainato M, Cabrini S, Munechika K. Nanoimprinted high-refractive index active photonic nanostructures based on quantum dots for visible light. Scientific Reports, 2017, 7(1): 17645
102. Guo L J. Nanoimprint lithography: methods and material requirements. Advanced Materials, 2007, 19(4): 495–513
103. Wang C, Shao J, Tian H, Li X, Ding Y, Li B Q. Step-controllable electric-field-assisted nanoimprint lithography for uneven large-area substrates. ACS Nano, 2016, 10(4): 4354–4363
104. Ahn S H, Guo L J. High-speed roll-to-roll nanoimprint lithography on flexible plastic substrates. Advanced Materials, 2008, 20(11): 2044–2049
105. Lee S H, Kim S W, Kang B S, Chang P S, Kwak M K. Scalable and continuous fabrication of bio-inspired dry adhesives with a thermosetting polymer. Soft Matter, 2018, 14(14): 2586–2593
106. Wong H C, Grenci G, Wu J, Viasnoff V, Low H Y. Roll-to-roll fabrication of residual-layer-free micro/nanoscale membranes with precise pore architectures and tunable surface textures. Industrial & Engineering Chemistry Research, 2018, 57(41): 13759–13768
107. Wang Z Z, Yi P Y, Peng L F, Lai X M, Ni J. Continuous fabrication of highly conductive and transparent Ag mesh electrodes for flexible electronics. IEEE Transactions on Nanotechnology, 2017, 16(4): 687–694
108. Yi P Y, Zhang C P, Peng L F, Lai X M. Flexible silver-mesh electrodes with moth-eye nanostructures for transmittance enhancement by double-sided roll-to-roll nanoimprint lithography. RSC Advances, 2017, 7(77): 48835–48840
109. Lee N, Yoo S, Kim C H, Lim J. Development of continuous metal patterns using two-dimensional atmospheric-pressure plasma-jet: On application to fabricate electrode on a flexible surface for film touch sensor. Journal of Micromechanics and Microengineering, 2019, 29(4): 045013
110. Wang L J, Zheng Y S, Wu C, Jia S L. Experimental investigation of photoresist etching by kHz AC atmospheric pressure plasma jet. Applied Surface Science, 2016, 385(1): 191–198
111. Zhou Y Q, Li M J, Shen L G, Ye H C, Wang J P, Huang S Z. Effect of resin accumulation on filling process in roll-to-roll UV imprint lithography. Journal of Vacuum Science & Technology B, Microelectronics and Nanometer Structures, 2017, 35(3): 031602
112. Tahir U, Kamran M A, Jeong M Y. Numerical study on the optimization of roll-to-roll ultraviolet imprint lithography. Coatings, 2019, 9(9): 573
113. Kotz F, Schneider N, Striegel A, Wolfschläger A, Keller N, Worgull M, Bauer W, Schild D, Milich M, Greiner C, Helmer D, Rapp B E. Glassomer-processing fused silica glass like a polymer. Advanced Materials, 2018, 30(22): e1707100
114. Leitgeb M, Nees D, Ruttloff S, Palfinger U, Götz J, Liska R, Belegratis M R, Stadlober B. Multilength scale patterning of functional layers by roll-to-roll ultraviolet-light-assisted nanoimprint lithography. ACS Nano, 2016, 10(5): 4926–4941
115. Koo S, Lee S H, Kim J D, Hong J G, Baac H W, Kwak M K, Ok J G. Controlled airbrush coating of polymer resists in roll-to-roll nanoimprinting with regimented residual layer thickness. International Journal of Precision Engineering and Manufacturing, 2016, 17(7): 943–947
116. Lee J H, Na M, Kim J, Yoo K, Park J, Kim J D, Oh D K, Lee S, Youn H, Kwak M K, Ok J G. Rapid and conformal coating of polymer resins by airbrushing for continuous and high-speed roll-to-roll nanopatterning: parametric quality controls and extended applications. Nano Convergence, 2017, 4(1): 11
117. Kodihalli Shivaprakash N, Ferraguto T, Panwar A, Banerjee S S, Barry C F, Mead J. Fabrication of flexible polymer molds for polymer microstructuring by roll-to-roll hot embossing. ACS Omega, 2019, 4(7): 12480–12488
118. Striegel A, Schneider M, Schneider N, Benkel C, Worgull M. Seamless tool fabrication for roll-to-roll microreplication. Microelectronic Engineering, 2018, 194(1): 8–14
119. Zhang X Q, Huang R, Liu K, Kumar A S, Shan X C. Rotating-tool diamond turning of Fresnel lenses on a roller mold for manufacturing of functional optical film. Precision Engineering,

2018, 51(1): 445–457

120. Lee Y H, Ke K C, Chang N W, Yang S Y. Development of an UV rolling system for fabrication of micro/nano structure on polymeric films using a gas-roller-sustained seamless PDMS mold. Microsystem Technologies, 2018, 24(7): 2941–2948
121. Lee C R, Ok J G, Jeong M Y. Nanopatterning on the cylindrical surface using an e-beam pre-mapping algorithm. Journal of Micromechanics and Microengineering, 2019, 29(1): 015004
122. Dumond J J, Low H Y, Lee H P, Fuh J Y H. Multi-functional silicone stamps for reactive release agent transfer in UV roll-to-roll nanoimprinting. Materials Horizons, 2016, 3(2): 152–160
123. Odom T W, Love J C, Wolfe D B, Paul K E, Whitesides G M. Improved pattern transfer in soft lithography using composite stamps. Langmuir, 2002, 18(13): 5314–5320
124. Kim S, Hyun S, Lee J, Lee K S, Lee W, Kim J K. Anodized aluminum oxide/polydimethylsiloxane hybrid mold for roll-to-roll nanoimprinting. Advanced Functional Materials, 2018, 28(23): 1800197
125. Ansari K, Kan J, Bettiol A A, Watt F. Stamps for nanoimprint lithography fabricated by proton beam writing and nickel electroplating. Journal of Micromechanics and Microengineering, 2006, 16(10): 1967–1974
126. Liu F, Tan K B, Malar P, Bikkarolla S K, van Kan J A. Fabrication of nickel molds using proton beam writing for micro/nano fluidic devices. Microelectronic Engineering, 2013, 102(1): 36–39
127. Lin X, Dou X, Wang X, Chen R T. Nickel electroplating for nanostructure mold fabrication. Journal of Nanoscience and Nanotechnology, 2011, 11(8): 7006–7010
128. Kwak M K, Ok J G, Lee S H, Guo L J. Visually tolerable tiling (VTT) for making a large-area flexible patterned surface. Materials Horizons, 2015, 2(1): 86–90
129. Ok J G, Ahn S H, Kwak M K, Guo L J. Continuous and high-throughput nanopatterning methodologies based on mechanical deformation. Journal of Materials Chemistry C, Materials for Optical and Electronic Devices, 2013, 1(46): 7681–7691
130. Ok J G, Shin Y J, Park H J, Guo L J. A step toward next-generation nanoimprint lithography: extending productivity and applicability. Applied Physics A, Materials Science & Processing, 2015, 121(2): 343–356
131. Ok J G, Park H J, Kwak M K, Pina-Hernandez C A, Ahn S H, Guo L J. Continuous patterning of nanogratings by nanochannel-guided lithography on liquid resists. Advanced Materials, 2011, 23(38): 4444–4448
132. Ahn S H, Guo L J. Dynamic nanoinscribing for continuous and seamless metal and polymer nanogratings. Nano Letters, 2009, 9 (12): 4392–4397
133. Oh D K, Nguyen D T, Lee S, Ko P, Heo G S, Yun C H, Ha T W, Youn H, Ok J G. Facile and scalable fabrication of flexible reattachable ionomer nanopatterns by continuous multidimensional nanoinscribing and low-temperature roll imprinting. ACS Applied Materials & Interfaces, 2019, 11(12): 12070–12076
134. Oh D K, Lee S, Lee S H, Lee W, Yeon G, Lee N, Han K S, Jung S, Kim D H, Lee D Y, Lee S H, Park H J, Ok J G. Tailored nanopatterning by controlled continuous nanoinscribing with tunable shape, depth, and dimension. ACS Nano, 2019, 13(10): 11194–11202
135. Ahn S H, Ok J G, Kwak M K, Lee K T, Lee J Y, Guo L J. Template-free vibrational indentation patterning (VIP) of micro/nanometer-scale grating structures with real-time pitch and angle tunability. Advanced Functional Materials, 2013, 23(37): 4739–4744
136. Ok J G, Panday A, Lee T, Jay Guo L. Continuous fabrication of scalable 2-dimensional (2D) micro- and nanostructures by sequential 1D mechanical patterning processes. Nanoscale, 2014, 6(24): 14636–14642
137. Ahiboz D, Manley P, Becker C. Adjustable large-area dielectric metasurfaces for near-normal oblique incident excitation. OSA Continuum, 2020, 3(4): 971–981
138. Zhu J, Wang Z, Lin S, Jiang S, Liu X, Guo S. Low-cost flexible plasmonic nanobump metasurfaces for label-free sensing of serum tumor marker. Biosensors & Bioelectronics, 2020, 150(1): 111905
139. Das Gupta T, Martin-Monier L, Yan W, Le Bris A, Nguyen-Dang T, Page A G, Ho K T, Yesilköy F, Altug H, Qu Y, Sorin F. Self-assembly of nanostructured glass metasurfaces via templated fluid instabilities. Nature Nanotechnology, 2019, 14(4): 320–327
140. Shneidman A V, Becker K P, Lukas M A, Torgerson N, Wang C, Reshef O, Burek M J, Paul K, McLellan J, Lončar M. All-polymer integrated optical resonators by roll-to-roll nanoimprint lithography. ACS Photonics, 2018, 5(5): 1839–1845
141. Zhang C, Yi P, Peng L, Lai X, Chen J, Huang M, Ni J. Continuous fabrication of nanostructure arrays for flexible surface enhanced Raman scattering substrate. Scientific Reports, 2017, 7(1): 39814
142. Suresh V, Ding L, Chew A B, Yap F L. Fabrication of large-area flexible SERS substrates by nanoimprint lithography. ACS Applied Nano Materials, 2018, 1(2): 886–893
143. Deng Y, Yi P, Peng L, Lai X, Lin Z. Experimental investigation on the large-area fabrication of micro-pyramid arrays by roll-to-roll hot embossing on PVC film. Journal of Micromechanics and Microengineering, 2014, 24(4): 045023
144. Højlund-Nielsen E, Clausen J, Mäkela T, Thamdrup L H, Zalkovskij M, Nielsen T, Li Pira N, Ahopelto J, Mortensen N A, Kristensen A. Plasmonic colors: toward mass production of metasurfaces. Advanced Materials Technologies, 2016, 1(7): 1600054
145. Murthy S, Pranov H, Feidenhans'l N A, Madsen J S, Hansen P E, Pedersen H C, Taboryski R. Plasmonic color metasurfaces fabricated by a high speed roll-to-roll method. Nanoscale, 2017, 9(37): 14280–14287
146. Ok J G, Youn H S, Kwak M K, Lee K T, Shin Y J, Guo L J, Greenwald A, Liu Y S. Continuous and scalable fabrication of flexible metamaterial films via roll-to-roll nanoimprint process for broadband plasmonic infrared filters. Applied Physics Letters, 2012, 101(22): 223102
147. Wi J S, Lee S, Lee S H, Oh D K, Lee K T, Park I, Kwak M K, Ok J G. Facile three-dimensional nanoarchitecturing of double-bent gold strips on roll-to-roll nanoimprinted transparent nanogratings for flexible and scalable plasmonic sensors. Nanoscale, 2017, 9(4): 1398–1402
148. Wi J S, Oh D K, Kwak M K, Ok J G. Size-dependent detection sensitivity of spherical particles sitting on a double-bent gold strip array. Optical Materials Express, 2018, 8(7): 1774–1779
149. Jeon S, Shir D J, Nam Y S, Nidetz R, Highland M, Cahill D G,

Rogers J A, Su M F, El-Kady I F, Christodoulou C G, Bogart G R. Molded transparent photopolymers and phase shift optics for fabricating three dimensional nanostructures. Optics Express, 2007, 15(10): 6358–6366

150. Choi J H, Oh C M, Jang J W. Micro- and nano-patterns fabricated by embossed microscale stamp with trenched edges. RSC Advances, 2017, 7(51): 32058–32064
151. Yanagishita T, Murakoshi K, Kondo T, Masuda H. Preparation of superhydrophobic surfaces with micro/nano alumina molds. RSC Advances, 2018, 8(64): 36697–36704
152. Kim S J, Jung P H, Kim W, Lee H, Hong S H. Generation of highly integrated multiple vivid colours using a three-dimensional broadband perfect absorber. Scientific Reports, 2019, 9(1): 14859
153. Jeong H E, Lee J K, Kim H N, Moon S H, Suh K Y. A nontransferring dry adhesive with hierarchical polymer nanohairs. Proceedings of the National Academy of Sciences of the United States of America, 2009, 106(14): 5639–5644
154. Karageorgiev P, Neher D, Schulz B, Stiller B, Pietsch U, Giersig M, Brehmer L. From anisotropic photo-fluidity towards nanomanipulation in the optical near-field. Nature Materials, 2005, 4(9): 699–703
155. Choi J, Cho W, Jung Y S, Kang H S, Kim H T. Direct fabrication of micro/nano-patterned surfaces by vertical-directional photofluidization of azobenzene materials. ACS Nano, 2017, 11(2): 1320–1327
156. Choi J, Jo W, Lee S Y, Jung Y S, Kim S H, Kim H T. Flexible and robust superomniphobic surfaces created by localized photofluidization of azopolymer pillars. ACS Nano, 2017, 11(8): 7821–7828
157. Liu Z, Cui Q, Huang Z, Guo L J. Transparent colored display enabled by flat glass waveguide and nanoimprinted multilayer gratings. ACS Photonics, 2020, 7(6): 1418–1424
158. Kothari R, Beaulieu M R, Hendricks N R, Li S, Watkins J J. Direct patterning of robust one-dimensional, two-dimensional, and three-dimensional crystalline metal oxide nanostructures using imprint lithography and nanoparticle dispersion inks. Chemistry of Materials, 2017, 29(9): 3908–3918
159. Li W, Zhou Y, Howell I R, Gai Y, Naik A R, Li S, Carter K R, Watkins J J. Direct imprinting of scalable, high-performance woodpile electrodes for three-dimensional lithium-ion nanobatteries. ACS Applied Materials & Interfaces, 2018, 10(6): 5447–5454
160. Liu D M, Wang Q K, Wang Q. Transfer the multiscale texture of crystalline Si onto thin-film micromorph cell by UV nanoimprint for light trapping. Applied Surface Science, 2018, 439(1): 168–175
161. Choi J, Jia Z, Park S. Fabrication of polymeric dual-scale nanoimprint molds using a polymer stencil membrane. Microelectronic Engineering, 2018, 199(1): 101–105
162. Han K S, Hong S H, Kim K I, Cho J Y, Choi K W, Lee H. Fabrication of 3D nano-structures using reverse imprint lithography. Nanotechnology, 2013, 24(4): 045304
163. Kwon Y W, Park J, Kim T, Kang S H, Kim H, Shin J, Jeon S, Hong S W. Flexible near-field nanopatterning with ultrathin, conformal phase masks on nonplanar substrates for biomimetic hierarchical photonic structures. ACS Nano, 2016, 10(4): 4609–4617
164. Wang C, Shao J, Lai D, Tian H, Li X. Suspended-template electric-assisted nanoimprinting for hierarchical micro-nanostructures on a fragile substrate. ACS Nano, 2019, 13(9): 10333–10342
165. Chandramohan A, Sibirev N V, Dubrovskii V G, Petty M C, Gallant A J, Zeze D A. Model for large-area monolayer coverage of polystyrene nanospheres by spin coating. Scientific Reports, 2017, 7(1): 40888
166. Nakagawa M, Nakaya A, Hoshikawa Y, Ito S, Hiroshiba N, Kyotani T. Size-dependent filling behavior of UV-curable di(meth) acrylate resins into carbon-coated anodic aluminum oxide pores of around 20 nm. ACS Applied Materials & Interfaces, 2016, 8(44): 30628–30634
167. Hua F, Sun Y G, Gaur A, Meitl M A, Bilhaut L, Rotkina L, Wang J F, Geil P, Shim M, Rogers J A, Shim A. Polymer imprint lithography with molecular-scale resolution. Nano Letters, 2004, 4 (12): 2467–2471
168. Yim W, Park S J, Han S Y, Park Y H, Lee S W, Park H J, Ahn Y H, Lee S, Park J Y. Carbon nanotubes as etching masks for the formation of polymer nanostructures. ACS Applied Materials & Interfaces, 2017, 9(50): 44053–44059
169. Pi S, Lin P, Xia Q. Fabrication of sub-10 nm metal nanowire arrays with sub-1 nm critical dimension control. Nanotechnology, 2016, 27(46): 464004
170. Woo J Y, Jo S, Oh J H, Kim J T, Han C S. Facile and precise fabrication of 10-nm nanostructures on soft and hard substrates. Applied Surface Science, 2019, 484(1): 317–325
171. Lim S H, Saifullah M S, Hussain H, Loh W W, Low H Y. Direct imprinting of high resolution TiO_2 nanostructures. Nanotechnology, 2010, 21(28): 285303
172. Menumerov E, Golze S D, Hughes R A, Neretina S. Arrays of highly complex noble metal nanostructures using nanoimprint lithography in combination with liquid-phase epitaxy. Nanoscale, 2018, 10(38): 18186–18194
173. Pina-Hernandez C, Fu P F, Guo L J. Ultrasmall structure fabrication via a facile size modification of nanoimprinted functional silsesquioxane features. ACS Nano, 2011, 5(2): 923–931
174. Yao Y H, Wang Y F, Liu H, Li Y R, Song B X, Wu W. Line width tuning and smoothening for periodical grating fabrication in nanoimprint lithography. Applied Physics A, Materials Science & Processing, 2015, 121(2): 399–403
175. Wang S S, Magnusson R. Theory and applications of guided-mode resonance filters. Applied Optics, 1993, 32(14): 2606–2613
176. Liu Z. One-step fabrication of crystalline metal nanostructures by direct nanoimprinting below melting temperatures. Nature Communications, 2017, 8(1): 14910
177. Bhadauriya S, Wang X, Pitliya P, Zhang J, Raghavan D, Bockstaller M R, Stafford C M, Douglas J F, Karim A. Tuning the relaxation of nanopatterned polymer films with polymer-grafted nanoparticles: observation of entropy-enthalpy compensation. Nano Letters, 2018, 18(12): 7441–7447
178. Liu L, Zhang Q, Lu Y S, Du W, Li B, Cui Y S, Yuan C S, Zhan P, Ge H X, Wang Z L, Chen Y F. A high-performance and low cost SERS substrate of plasmonic nanopillars on plastic film fabricated by nanoimprint lithography with AAO template. AIP Advances, 2017, 7(6): 065205
179. Jung Y, Hwang I, Yu J, Lee J, Choi J H, Jeong J H, Jung J Y, Lee J.

Fano metamaterials on nanopedestals for plasmon-enhanced infrared spectroscopy. Scientific Reports, 2019, 9(1): 7834
180. Yao Y H, Wu W. All-dielectric heterogeneous metasurface as an efficient ultra-broadband reflector. Advanced Optical Materials, 2017, 5(14): 1700090
181. Hemmati H, Magnusson R. Resonant dual-grating metamembranes supporting spectrally narrow bound states in the continuum. Advanced Optical Materials, 2019, 7(20): 1900754
182. Zhang C, Subbaraman H, Li Q, Pan Z, Ok J G, Ling T, Chung C J, Zhang X, Lin X, Chen R T, Guo L J. Printed photonic elements: nanoimprinting and beyond. Journal of Materials Chemistry C, Materials for Optical and Electronic Devices, 2016, 4(23): 5133–5153
183. Lee K T, Jang J Y, Park S J, Ji C G, Yang S M, Guo L J, Park H J. Angle-insensitive and CMOS-compatible subwavelength color printing. Advanced Optical Materials, 2016, 4(11): 1696–1702
184. Liu H, Yang H, Li Y R, Song B X, Wang Y F, Liu Z R, Peng L, Lim H, Yoon J, Wu W. Switchable all-dielectric metasurfaces for full-color reflective display. Advanced Optical Materials, 2019, 7 (8): 1801639
185. Joo W J, Kyoung J, Esfandyarpour M, Lee S H, Koo H, Song S, Kwon Y N, Song S H, Bae J C, Jo A, Kwon M J, Han S H, Kim S H, Hwang S, Brongersma M L. Metasurface-driven OLED displays beyond 10000 pixels per inch. Science, 2020, 370 (6515): 459–463
186. Yoon G, Kim K, Kim S U, Han S, Lee H, Rho J. Printable nanocomposite metalens for high-contrast near-infrared imaging. ACS Nano, 2021, 15(1): 698–706
187. Checcucci S, Bottein T, Gurioli M, Favre L, Grosso D, Abbarchi M. Multifunctional metasurfaces based on direct nanoimprint of titania sol-gel coatings. Advanced Optical Materials, 2019, 7(10): 1801406
188. Kim K, Yoon G, Baek S, Rho J, Lee H. Facile nanocasting of dielectric metasurfaces with sub-100 nm resolution. ACS Applied Materials & Interfaces, 2019, 11(29): 26109–26115
189. Yoon G, Kim K, Huh D, Lee H, Rho J. Single-step manufacturing of hierarchical dielectric metalens in the visible. Nature Communications, 2020, 11(1): 2268
190. Gopalan K K, Paulillo B, Mackenzie D M A, Rodrigo D, Bareza N, Whelan P R, Shivayogimath A, Pruneri V. Scalable and tunable periodic graphene nanohole arrays for mid-infrared plasmonics. Nano Letters, 2018, 18(9): 5913–5918
191. Zhao Z J, Lee M, Kang H, Hwang S, Jeon S, Park N, Park S H, Jeong J H. Eight inch wafer-scale flexible polarization-dependent color filters with Ag-TiO_2 composite nanowires. ACS Applied Materials & Interfaces, 2018, 10(10): 9188–9196
192. Driencourt L, Federspiel F, Kazazis D, Tseng L T, Frantz R, Ekinci Y, Ferrini R, Gallinet B. Electrically tunable multicolored filter using birefringent plasmonic resonators and liquid crystals. ACS Photonics, 2020, 7(2): 444–453
193. Shin Y J, Pina-Hernandez C, Wu Y K, Ok J G, Guo L J. Facile route of flexible wire grid polarizer fabrication by angled-evaporations of aluminum on two sidewalls of an imprinted nanograting. Nanotechnology, 2012, 23(34): 344018
194. Matricardi C, Garcia-Pomar J L, Molet P, Perez L A, Alonso M I, Campoy-Quiles M, Mihi A. High-throughput nanofabrication of metasurfaces with polarization-dependent response. Advanced Optical Materials, 2020, 8(20): 2000786
195. Yoon G, Kim K, Kim S U, Han S, Lee H, Rho J. Printable nanocomposite metalens for high-contrast near-infrared imaging. ACS Nano, 2021, 15(1): 698–706
196. Yang Y, Yoon G, Park S, Namgung S D, Badloe T, Nam K T, Rho J. Revealing structural disorder in hydrogenated amorphous silicon for a low-loss photonic platform at visible frequencies. Advanced Materials, 2021, 33(9): e2005893
197. Oh D K, Jeong H, Kim J, Kim Y, Kim I, Ok J G, Rho J. Top-down nanofabrication approaches toward single-digit-nanometer scale structures. Journal of Mechanical Science and Technology, 20201, 35(3): 837–859
198. Stolt T, Kim J, Héron S, Vesala A, Yang Y, Mun J, Kim M, Huttunen M J, Czaplicki R, Kauranen M, Rho J, Genevet P. Backward phase-matched second-harmonic generation from stacked metasurfaces. Physical Review Letters, 2021, 126(3): 033901
199. Lee D, Go M, Kim M, Jang J, Choi C, Kim J K, Rho J. Multiple-patterning colloidal lithography-implemented scalable manufacturing of heat-tolerant titanium nitride broadband absorbers in the visible to near-infrared. Microsystems & Nanoengineering, 2021, 7(1): 14
200. Kim I, Ansari M A, Mehmood M Q, Kim W S, Jang J, Zubair M, Kim Y K, Rho J. Stimuli-responsive dynamic metaholographic displays with designer liquid crystal modulators. Advanced Materials, 2020, 32(50): e2004664
201. Chen Y, Ai B, Wong Z J. Soft optical metamaterials. Nano Convergence, 2020, 7(1): 18
202. Naveed M A, Ansari M A, Kim I, Badloe T, Kim J, Oh D K, Riaz K, Tauqeer T, Younis U, Saleem M, Anwar M S, Zubair M, Mehmood M Q, Rho J. Optical spin-symmetry breaking for high-efficiency directional helicity-multiplexed metaholograms. Microsystems & Nanoengineering, 2021, 7(1): 5

Dong Kyo Oh obtained his B.S. (2017) and M.S. (2019) degrees in Mechanical and Automotive Engineering from Seoul National University of Science and Technology (SEOULTECH), Republic of Korea. Currently, he is a Ph.D. student in Mechanical Engineering at Pohang University of Science and Technology (POSTECH), Republic of Korea. His research is mainly focused on flat optics based on metasurfaces, nanofabrication of metamaterials, and alternative nanofabrication.

Taejun Lee obtained his B.S. degree in Mechanical Engineering from Gachon University, Republic of Korea, in 2017. He is currently an M.S./Ph.D. integrated student in Mechanical Engineering at POSTECH, Republic of Korea. His research interest is novel lithography and dielectric metasurfaces.

Byoungsu Ko obtained his B.S. degree in Mechanical Engineering from Myongji University, Republic of Korea, in 2019. Currently, he is an M.S./Ph.D. integrated student in Mechanical Engineering at POSTECH, Republic of Korea. His research interests focus on nanofabrication and tunable metasurfaces.

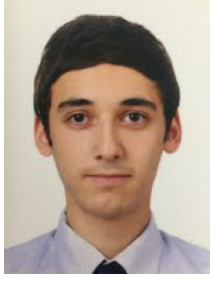

Trevon Badloe obtained his M.Phys. (hons) degree (2012) from The University of Sheffield, United Kingdom with one-year study abroad at National University of Singapore, Singapore (2010). After three years of teaching courses in English and classical mechanics as an assistant professor at Yeungjin University, Republic of Korea, he started working towards his Ph.D. in Mechanical Engineering at POSTECH, Republic of Korea (2017). His research interests include tunable metamaterials and metasurfaces, and machine learning for the design and optimization of nanophotonic applications.

Jong G. Ok is currently an associate professor in the Department of Mechanical and Automotive Engineering at SEOULTECH, Republic of Korea. He received his B.S. (2002) and M.S. (2007) degrees in Mechanical and Aerospace Engineering from Seoul National University, Republic of Korea, and Ph.D. (2013) degree in Mechanical Engineering from the University of Michigan, USA. His research focuses on smart and scalable nanomanufacturing and multiscale hybrid nanoarchitecturing.

Junsuk Rho is currently a Mu-En-Jae endowed chair associate professor with a joint appointment in Mechanical Engineering and Chemical Engineering at POSTECH, Republic of Korea. He received his B.S. (2007), M.S (2008), Ph.D. (2013) degrees all in Mechanical Engineering from Seoul National University, University of Illinois, Urbana-Champaign, University of California, Berkeley, respectively. His research is focused on developing novel nanophotonic materials and devices based on fundamental physics and experimental studies of deep subwavelength light-matter interaction.